

A PRIORI AND A POSTERIORI ERROR ESTIMATES OF A REALLY PRESSURE-ROBUST VIRTUAL ELEMENT METHOD FOR THE INCOMPRESSIBLE BRINKMAN EQUATIONS

YU XIONG[†] AND YANPING CHEN^{*}

Abstract. This paper presents both a priori and a posteriori error analyses for a really pressure-robust virtual element method to approximate the incompressible Brinkman problem. We construct a divergence-preserving reconstruction operator using the Raviart–Thomas element for the discretization on the right-hand side. The optimal priori error estimates are carried out, which imply the velocity error in the energy norm is independent of both the continuous pressure and the viscosity. Taking advantage of the virtual element method’s ability to handle more general polygonal meshes, we implement effective mesh refinement strategies and develop a residual-type a posteriori error estimator. This estimator is proven to provide global upper and local lower bounds for the discretization error. Finally, some numerical experiments demonstrate the robustness, accuracy, reliability and efficiency of the method.

Key words. Brinkman equations, virtual element, pressure-robust, priori and posteriori errors, adaptive mesh refinement

AMS subject classifications. 65N15, 65N30, 76D07, 35J47, 35K55

1. Introduction. This paper is concerned with the development of robust virtual element numerical methods for the Brinkman equations. The Brinkman equations model fluid flow in complex porous media with a permeability coefficient highly varying so that the flow is dominated by Darcy in some regions and by Stokes in others. In a simple form, the Brinkman model seeks unknown velocity \mathbf{u} and pressure p satisfying

$$\begin{aligned} (1.1a) \quad & -\nu \Delta \mathbf{u} + \nu \kappa^{-1} \mathbf{u} - \nabla p = \mathbf{f} & \text{in } \Omega, \\ (1.1b) \quad & \nabla \cdot \mathbf{u} = 0 & \text{in } \Omega, \\ (1.1c) \quad & \mathbf{u} = \mathbf{0} & \text{on } \partial\Omega. \end{aligned}$$

Here, $\nu > 0$ and \mathbf{f} denote the fluid viscosity and source term, respectively. The permeability tensor κ of the porous media is symmetric positive definite.

The incompressible Brinkman equations, as given by equations (1.1a) and (1.1b), model fluid flow in fractured porous media. They can be seen as a generalization of the Stokes equations, which approximate the Navier–Stokes equations at low Reynolds numbers. This modeling is crucial for studying fluid dynamics in porous media, with significant implications for industrial and environmental issues such as industrial filters and open foams [33]. The permeability, which varies greatly, causes flow velocity to change substantially through the porous medium. Mathematically, the Brinkman equations combine

* Corresponding author. School of Science, Nanjing University of Posts and Telecommunications, Nanjing 210023, China. (Email:yanpingchen@njupt.edu.cn)

† School of Mathematics and Computational Science, Hunan Key Laboratory for Computation and Simulation in Science and Engineering, Xiangtan University, Xiangtan, 411105, Hunan, China. (Email:xiongyu@smail.xtu.edu.cn)

This work is supported by the State Key Program of National Natural Science Foundation of China (11931003), Natural Science Research Start-up Foundation of Recruiting Talents of Nanjing University of Posts and Telecommunications (NY223127) and Postgraduate Scientific Research Innovation Foundation of Xiangtan University (XDCX2024Y178).

features of both the Stokes and Darcy equations, with the type of flow changing across the computational domain. In regions with high permeability κ , the model behaves like the Stokes equations, while in areas with low permeability κ , it simplifies to the Darcy equations. Therefore, numerical schemes for the Brinkman equations must be carefully designed to handle both Stokes and Darcy flows, which is essential for accurately simulating fluid flow in porous media. To address these challenges, various strategies have been proposed by researchers. In works such as [8], [9] and [43], Burman and Xie et al. have introduced jumps penalization techniques. These methods stabilize the Crouzeix-Raviart-P0 finite elements or P1-P0 finite elements by penalizing the normal component of the velocity field or the pressure field, respectively. It is worth mentioning that most of the numerical methods for solving Brinkman equations are rely on triangular (simplicial) and quadrilateral meshes. However, there exists another numerical methods that offers great flexibility in meshing with polygonal elements, such as weak Galerkin method (WG), mimetic finite differences method (MFD) and virtual element method (VEM). In particular, Mu et al. [33] developed a stable weak Galerkin finite element method that provides a robust and accurate numerical scheme for both Darcy and Stokes dominated flows. Furthermore, Zhai et al. [47] presented a new weak Galerkin finite element scheme for the model, which offers a flexible and efficient approach to solve the Brinkman equations in complex porous media by utilizing generalized functions and their weak derivatives.

As a generalization of the finite element method (FEM) and mimetic finite differences method on polygonal mesh, the virtual element method was initially proposed by Beirão da Veiga et al. [15, 17] and has attracted the attention of many researchers in recent years. The construction of the virtual element space involves a combination of a polynomial subspace and an additional non-polynomial virtual subspace. To approximate the non-polynomial parts of the discrete bilinear forms, suitable projection operators are employed, which rely only on the degrees of freedom linked to the virtual element space. Consequently, we can effectively handle meshes with more general polygonal elements, without the need for directly calculating non-polynomial functions. For a thorough description of the VEM, see [2, 16, 29]. In recent years, the VEM has attracted more and more researchers' attention to solve fluid flow problems, such as the Stokes problem [12, 19, 21, 30], the Navier-Stokes problem [23, 25], the Darcy-Stokes problem [48, 49] and so on [13, 18, 22, 31, 40]. As we discussed in previous work [44], the VEM basis functions are closely related to the partial differential equation (PDE) within each element, facilitating the construction of divergence-free virtual elements. Although divergence-free VEM have been developed to solve the Brinkman problem [35], it is not really pressure-robust due to the fact that the right-hand side term is not carefully discretized [21]. In the standard divergence-free VEM scheme, this consistency error enters the prior velocity estimate as the inverse of the viscosity $1/\nu$, so locking phenomenon occurs when $\nu \rightarrow 0$. A significant contribution in the VEM approximate to the Brinkman equations was made by Wang et al. [39], who developed a really pressure-robust VEM scheme by constructing a divergence-preserving CW_0 reconstruction operator. Moreover, the reconstruction technique has also been applied to the conforming VEM [37, 41] and nonconforming VEM [26, 27] for (Navier-) Stokes problems. Inspired by the aforementioned works, we will construct a virtual element based on divergence-preserving Raviart-Thomas reconstruction operator to solve the Brinkman problem. From a computational perspective, in practical applications, the lowest-order virtual element is typically preferred, and our method is also applicable for the case $k = 1$.

On the other hand, in numerical approximate to PDE problems, it is crucial to use adaptive mesh refinement techniques guided by a posteriori error indicators. For instance, they ensure that the errors remain beneath a specified threshold at a reasonable computational expense, particularly when dealing with solutions that exhibit singular behavior. Due to the large flexibility of the meshes to which the VEM is applied, mesh adaptivity becomes an appealing feature since mesh refinement strategies can be

implemented very efficiently. The field of a posteriori error analysis for the VEM has seen significant development. Beirão da Veiga et al. [5] firstly developed a residual-based a posteriori error estimator for the C^1 -conforming VEM applied to the Poisson problem. After that they focused on a posteriori error estimation for mesh adaptivity within the hp-VEM framework [6]. Moreover, Chi et al. [14] introduced a recovery-based a posteriori error estimation framework that is applicable to VEMs of any order. Lastly, some residual-type posteriori error estimators for the virtual element approximation of the (Navier-) Stokes problem are presented in [28, 38, 42]. It is natural that we develop an adaptive VEM algorithm guided by a residual-type a posteriori error estimator for the Brinkman equation (1.1).

The aim of this paper is to develop a really pressure-robust and divergence-free VEM for the two-dimensional incompressible Brinkman problem. In addition to deriving the optimal a priori error estimate, we also give a posterior error estimator and prove its reliability and efficiency. It is noteworthy that, in contrast to the standard divergence-free VEM scheme, the velocity error within the prior error estimation is independent not only of the continuous pressure p but also of the viscosity ν , thereby achieving really pressure robustness. The paper also proves the well-posedness of the proposed VEM scheme. Numerical experiments not only validate our theoretical analyses, but also conduct robust and reliable flow simulations in two types of porous media regions with high contrast permeability.

The structure of this paper is outlined as follows: Section 2 explains essential notations, derives the weak formulation of the Brinkman equations, and introduces the Helmholtz decomposition. In Section 3, a framework of a really pressure-robust VEM is constructed and the presented scheme is proven to be well-posed. The optimal a posteriori error estimate is derived in Section 4. Section 5 present a accurate and effective posteriori error estimator driving the adaptive mesh refinement. In Section 6, we implement some numerical experiments. Finally, we offer our conclusions in Section 7.

2. Notations and Preliminaries. We consider a convex polygonal domain Ω within the two-dimensional Euclidean space \mathbb{R}^2 , characterized by a Lipschitz boundary $\partial\Omega$. The $L^2(\Omega)$ norm and inner product will be denoted by $\|\cdot\|$ and (\cdot, \cdot) , respectively, while all other norms will be labeled with subscripts or specifically defined.

Then we consider the natural functions spaces for velocity and pressure, respectively, by

$$\mathbf{V} := [H_0^1(\Omega)]^2 \quad \text{and} \quad Q := L_0^2(\Omega) = \{q \in L^2(\Omega) : (q, 1) = 0\},$$

where the space \mathbf{V} equipped with the energy norm

$$(2.1) \quad \|\mathbf{v}\| := \left(\|\nabla \mathbf{v}\|^2 + \|\kappa^{-1/2} \mathbf{v}\|^2 \right)^{\frac{1}{2}} \quad \forall \mathbf{v} \in \mathbf{V},$$

where the permeability κ is defined in (1.1). In \mathbf{V} , we have the Friedrichs inequality: there exists a constant C_F depending only on Ω such that for any $\Phi \in \mathbf{V}$,

$$(2.2) \quad \|\Phi\|_1 \leq C_F \|\nabla \Phi\|.$$

Moreover, we introduce the kernel space

$$(2.3) \quad \mathbf{Z} := \{\mathbf{v} \in \mathbf{V} \text{ s.t. } (\nabla \cdot \mathbf{v}, q) = 0 \text{ for all } q \in Q\}.$$

2.1. The continuous problem. Based on the above preliminaries, the variational formulation of problem (1.1) is: find $(\mathbf{u}, p) \in \mathbf{V} \times Q$ such that

$$(2.4a) \quad \nu a(\mathbf{u}, \mathbf{v}) + b(\mathbf{v}, p) = (\mathbf{f}, \mathbf{v}) \quad \forall \mathbf{v} \in \mathbf{V},$$

$$(2.4b) \quad b(\mathbf{u}, q) = 0 \quad \forall q \in Q,$$

where the continuous bilinear forms are defined as

$$a(\mathbf{u}, \mathbf{v}) := \int_{\Omega} \nabla \mathbf{u} : \nabla \mathbf{v} + \kappa^{-1} \mathbf{u} \cdot \mathbf{v} \, dx, \quad b(\mathbf{v}, q) := \int_{\Omega} q \nabla \cdot \mathbf{v} \, dx,$$

where the bilinear form $b(\cdot, \cdot)$ and the space \mathbf{V} and Q satisfy the inf-sup condition [7], i.e., \exists constant γ such that

$$(2.5) \quad \sup_{\mathbf{v} \in \mathbf{V}, \mathbf{v} \neq 0} \frac{b(\mathbf{v}, q)}{\|\nabla \mathbf{v}\|} \geq \gamma \|q\| \quad \forall q \in Q.$$

It is obvious that the bilinear form $a(\cdot, \cdot)$ is continuous and coercive: there exists a positive constant C_a such that

$$(2.6a) \quad a(\mathbf{w}, \mathbf{v}) \leq C_a \|\mathbf{w}\| \|\mathbf{v}\| \quad \forall \mathbf{w}, \mathbf{v} \in \mathbf{V}.$$

$$(2.6b) \quad a(\mathbf{v}, \mathbf{v}) \geq \|\mathbf{v}\|^2 \quad \forall \mathbf{v} \in \mathbf{V}.$$

Combining (2.5), (2.6b) and the standard saddle point theory, [39] one can get the well-posedness of the continue problem (2.4).

2.2. The Helmholtz decomposition. For the load term $\mathbf{f} \in [L^2(\Omega)]^2$, there exists a unique Helmholtz decomposition [24]

$$(2.7) \quad \mathbf{f} = \mathbb{P}(\mathbf{f}) + \nabla \alpha,$$

where $\mathbb{P}(\mathbf{f}) \in \{\mathbf{v} \in [L^2(\Omega)]^2 : \nabla \cdot \mathbf{v} = 0, \mathbf{v} = 0 \text{ on } \partial\Omega\}$ is called the Helmholtz projector of \mathbf{f} and $\alpha \in H^1(\Omega)$. Then by restricting $\mathbf{v} \in \mathbf{Z}$, the weak form (2.4) can be reformulated as the divergence-free problem: find $\mathbf{u} \in \mathbf{Z}$ such that

$$(2.8) \quad \nu a(\mathbf{u}, \mathbf{v}) = (\mathbb{P}(\mathbf{f}), \mathbf{v}) \quad \forall \mathbf{v} \in \mathbf{Z}.$$

Furthermore, choosing $\mathbf{v} = \mathbf{u}$, combining (2.6b) and the Poincaré inequality with the constant C_P , we have

$$\nu \|\mathbf{u}\|^2 = \nu a(\mathbf{u}, \mathbf{u}) = (\mathbb{P}(\mathbf{f}), \mathbf{u}) \leq C_P \|\mathbb{P}(\mathbf{f})\| \cdot \|\mathbf{u}\| \leq C_P \|\mathbb{P}(\mathbf{f})\| \|\mathbf{u}\|,$$

where the last step follows naturally, due to the fact that κ is symmetric positive definite. Then we obtain the stability estimate for the velocity

$$(2.9) \quad \|\mathbf{u}\| \leq \frac{C_P}{\nu} \|\mathbb{P}(\mathbf{f})\|.$$

3. A really pressure-robust Virtual element. In this section, we introduce the concept of polygonal subdivision of Ω and the basic settings of the VEM. Subsequently, we constructed a divergence-preserving reconstruction operator based on the lowest-order Raviart-Thomas finite element space RT_0 , and applied it to the discretization of the right-hand side, thereby proposing a really pressure-robust and well-posed VEM scheme.

3.1. Projection operators and virtual element spaces. Let $\{\Omega_h\}$ represent the sequence of Ω subdivided into a set of general polygonal elements E with $h_E := \text{diameter}(E)$, mesh size $h := \max_{E \in \Omega_h} h_E$ and boundary ∂E . Moreover, e stands for a generic edge of an element E ; N_E^V denotes the number of vertices in E , and V_i , $1 \leq i \leq N_E^V$ represent any vertex in E . We also denote the outward unit normal vector and unit tangential vector on ∂E by \mathbf{n}_E and \mathbf{t}_E , respectively. The subscript E will be dropped in a clear space. Moreover, denote by \mathcal{E}_e the set of elements taking e as an edge, and let \mathcal{F}_h^0 be a set of interior edge shared by two elements. We suppose that $\{\Omega_h\}$ satisfy the following assumptions (refer [15, 17, 36, 44]):

ASSUMPTION 3.1. *There exists a positive real number ρ such that for all h and for every $E \in \Omega_h$:*
(1) *the ratio between the shortest edge e_{\min} and the diameter h_E of E is greater than ρ , i.e., $\frac{e_{\min}}{h_E} > \rho$;*
(2) *E is star-shaped with respect to a ball of radius ρh_E and center $\mathbf{x}_E \in E$.*

For any non-negative integer k , $P_k(\mathcal{D})$ denotes the space of polynomials with total degree less than or equal to k on the bounded domain \mathcal{D} of dimension d ($d = 1, 2$), as an edge or an element, and the corresponding vector polynomial space denotes as $\mathbf{P}_k(\mathcal{D})$. Let $\mathbf{x}_{\mathcal{D}}$ and $h_{\mathcal{D}}$ be denoted as the barycenter and the diameter of \mathcal{D} , respectively. We denote by $\mathcal{M}_k(\mathcal{D})$ the scaled monomial set as a basis for the polynomial space $\mathbf{P}_k(\mathcal{D})$ defined on \mathcal{D} [1, 15, 17]. The set of scaled monomials $\mathcal{M}_k(\mathcal{D})$ with degrees less than or equal to k is defined as follows

$$\mathcal{M}_k(\mathcal{D}) := \left\{ m : m = \left(\frac{\mathbf{x} - \mathbf{x}_{\mathcal{D}}}{h_{\mathcal{D}}} \right)^{\alpha} \quad \text{for } \alpha \in \mathbb{N}^d, 0 \leq |\alpha| \leq k \right\}.$$

For simplicity, we also define the following spaces

- $\mathcal{G}_k(E) := \nabla P_{k+1}(E) \subseteq \mathbf{P}_k(E)$;
- $\mathcal{G}_k^{\perp}(E) := \mathbf{x}^{\perp} P_{k-1}(E) \subseteq \mathbf{P}_k(E)$ with $\mathbf{x}^{\perp} = (y, -x)^T$;
- $\mathbf{B}_1(\partial E) := \{ \mathbf{v} \in \mathbf{C}^0(\partial E), \mathbf{v}|_e \cdot \mathbf{n}_E \in P_2(e), \mathbf{v}|_e \cdot \mathbf{t}_E \in P_1(e) \quad \forall e \in \partial E \}$.

Following [13, 36, 37], we introduce the local lowest order virtual element space for the velocity as follows:

$$\mathbf{U}_E := \left\{ \mathbf{v} \in \mathbf{H}^1(E) : \mathbf{v}|_{\partial E} \in \mathbf{B}_1(\partial E), \Delta \mathbf{v} - \nabla s = \mathbf{0} \text{ and } \nabla \cdot \mathbf{v} \in P_0(E) \right. \\ \left. \text{for some } s \in L_0^2(E) \right\}.$$

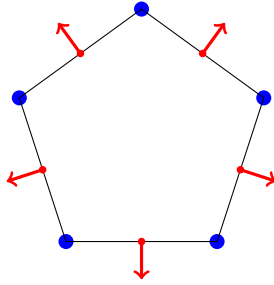


Fig. 3.1: Illustration of degrees of freedom. We represent $\mathbf{Dv1}$ with the blue dots, $\mathbf{Dv2}$ with the red arrows.

Correspondingly, as illustrated in Fig. 3.1, the degrees of freedom \mathbf{D}_V for local space \mathbf{U}_E include the following:

(3.1a) $\mathbf{D}_V 1:$ the values of \mathbf{v} at the vertices of the polygon E ,

$$(3.1b) \quad \mathbf{D}_V 2: \frac{1}{|e|} \int_e \mathbf{v} \cdot \mathbf{n} ds \quad \forall e \in \partial E.$$

Prior to defining the global virtual element spaces, we must first define two essential projection operators that ensure the computability of discrete linear forms. For any $\mathbf{v} \in \mathbf{U}_E$, an energy projection $\Pi^{\nabla, E}$ onto $\mathbf{P}_1(E)$ is defined by

$$(3.2a) \quad (\nabla(\mathbf{v} - \Pi^{\nabla, E}\mathbf{v}), \nabla \mathbf{p}_1)_E = 0 \quad \forall \mathbf{p}_1 \in \mathbf{P}_1(E),$$

$$(3.2b) \quad P^{0, E}(\Pi^{\nabla, E}\mathbf{v} - \mathbf{v}) = 0,$$

where the projector $P^{0, E}\mathbf{v} := \frac{1}{N_E^V} \sum_{i=1}^{N_E^V} \mathbf{v}(V_i)$ is onto the space of constants. It is obvious that $\Pi^{\nabla, E}\mathbf{p}_1 = \mathbf{p}_1$ holds for any $\mathbf{p}_1 \in \mathbf{P}_1(E)$.

REMARK 3.1. (The computability of $\Pi^{\nabla, E}$) By integrating by parts we can know that the term $(\nabla \mathbf{v}, \nabla \mathbf{p}_1)_E = (\mathbf{v}, \nabla \mathbf{p}_1 \cdot \mathbf{n}_E)_{\partial E}$, where $\nabla \mathbf{p}_1 \cdot \mathbf{n}_E$ is obviously a constant vector. And there exists a decomposition $\mathbf{v} = (\mathbf{v} \cdot \mathbf{n}_E)\mathbf{n}_E + (\mathbf{v} \cdot \mathbf{t}_E)\mathbf{t}_E$ on boundary ∂E . On the one hand, since $\mathbf{v} \cdot \mathbf{n}_E \in P_2(e)$ for $e \in \partial E$, we can easily calculate its integral on each edge, relying solely on the degrees of freedom (3.1a)-(3.1b). On the other hand, since $\mathbf{v} \cdot \mathbf{t}_E \in P_1(e)$ for $e \in \partial E$, we can easily calculate its integral on each edge by the trapezoidal rule and the vertex degrees of freedom (3.1a). Then the integral in (3.2a) is ordinary.

We proceed to define a local \mathbf{L}^2 -projection operator $\Pi^{0, E}$ from \mathbf{U}_E onto $\mathbf{P}_1(E)$, which is defined by

$$(3.3) \quad (\Pi^{0, E}\mathbf{v} - \mathbf{v}, \mathbf{p}_1)_E = 0 \quad \forall \mathbf{p}_1 \in \mathbf{P}_1(E),$$

Clearly, the two projection operators possess the subsequent estimations

$$(3.4a) \quad \|\Pi^{0, E}\mathbf{v}\|_E \leq \|\mathbf{v}\|_E,$$

$$(3.4b) \quad |\Pi^{\nabla, E}\mathbf{v}|_{1, E} \leq |\mathbf{v}|_{1, E}.$$

It is evident that the term $(\mathbf{v}, \mathbf{p}_1)_E$ is uncomputable for any $\mathbf{v} \in \mathbf{U}_E$. This observation has prompted us to define a modified space in which $(\mathbf{v}, \mathbf{p}_1)_E$ becomes computable. With the help of enhanced technology [1], we first enlarge the space \mathbf{U}_E to be

$$\widehat{\mathbf{U}}_E := \left\{ \mathbf{v} \in \mathbf{H}^1(E) : \mathbf{v}|_{\partial E} \in \mathbf{B}_1(\partial E), \Delta \mathbf{v} - \nabla s \in \mathcal{G}_1^\perp(E) \text{ and } \nabla \cdot \mathbf{v} \in P_0(E) \right. \\ \left. \text{for some } s \in L^2(E) \right\}.$$

We subsequently define the local virtual element space \mathbf{V}_E as the restriction of $\widehat{\mathbf{U}}_E$ given by

$$(3.5) \quad \mathbf{V}_E := \left\{ \mathbf{v} \in \widehat{\mathbf{U}}_E : (\mathbf{v} - \Pi_E^\nabla \mathbf{v}, \mathbf{p}_1)_E = 0 \text{ for any } \mathbf{p}_1 \in \mathcal{G}_1^\perp(E) \right\}.$$

As mentioned in [1, 41, 44], the dimension of \mathbf{V}_E is equal to that of original space \mathbf{U}_E , and these two spaces share the same degrees of freedom (3.1).

REMARK 3.2. (The computability of $\Pi^{0,E}$) For any $\mathbf{p}_1 \in \mathbf{P}_1(E)$, there exists a unique decomposition $\mathbf{p}_1 = \nabla s + \mathbf{g}$, where $s \in P_2(E)$ and $\mathbf{g} \in \mathcal{G}_1^\perp(E)$. Furthermore, the constant $\nabla \cdot \mathbf{v} \in P_0(E)$ can be readily computed using the divergence theorem along with the normal degree of freedom (3.1b). As demonstrated in the work [37], it is straightforward to explicitly express $\mathbf{v}|_e \cdot \mathbf{n}$ and $\mathbf{v}|_e \cdot \mathbf{t}$ on edge e , relying only on the degrees of freedom (3.1a)-(3.1b). It follows from integration by parts and the definition of $\Pi^{\nabla,E}$ that

$$(\mathbf{v}, \mathbf{p}_1)_E = (\mathbf{v}, \nabla s + \mathbf{g})_E = -(\nabla \cdot \mathbf{v}, s)_E + (\mathbf{v} \cdot \mathbf{n}, s)_{\partial E} + (\Pi^{\nabla,E} \mathbf{v}, \mathbf{g})_E,$$

whose right-hand side is evidently computable by using the computable $\nabla \cdot \mathbf{v}$ and $\Pi^{\nabla,E} \mathbf{v}$ within E and $\mathbf{v}|_{\partial E} \cdot \mathbf{n}$ on ∂E . Thereby the integral in (3.3) is ordinary. Finally, the global virtual element space for velocity is constructed by assembling the local spaces \mathbf{V}_E as follows:

$$\mathbf{V}_h := \{\mathbf{v} \in \mathbf{H}_0^1(\Omega) : \mathbf{v} \in \mathbf{V}_E \quad \forall E \in \mathcal{T}_h\}.$$

Moreover, the approximated space Q_h for the pressure is defined as the piecewise constant space, denoted by

$$(3.6) \quad Q_h := \{q \in L_0^2(\Omega) : q \in P_0(E) \quad \forall E \in \mathcal{T}_h\}.$$

We define the exact discrete kernel space \mathbf{Z}_h by utilizing the fact that $\nabla \cdot \mathbf{V}_h \subset Q_h$, as follows:

$$(3.7) \quad \mathbf{Z}_h := \{\mathbf{v}_h \in \mathbf{V}_h : b(\mathbf{v}_h, q_h) = 0 \quad \forall q_h \in Q_h\} = \{\mathbf{v}_h \in \mathbf{V}_h : \nabla \cdot \mathbf{v}_h = 0\}.$$

3.2. Divergence-preserving reconstruction operator. For each element $E \in \Omega_h$, we assume the existence of a subtriangulation that subdivides E into n_t regular triangles, with n_t is a constant correspond to E . A constrained Delaunay triangulation of the polygon yields a conforming simplicial submesh Ω_h^* relative to Ω_h , with each triangle $T \subset \Omega_h^*$ uniquely corresponding to an element $E \in \Omega_h$ ($T \subset E$), and each $E \in \Omega_h$ composed of several triangles from Ω_h^* . Consider polygon E with vertices V_i (for $i = 1, \dots, N_E^V$), ordered counterclockwise. Let \mathbf{n}_i^∂ denote the outward unit normal on edge e_i^∂ from V_i to V_{i+1} . Using modulus N_E^V indexing, E is triangulated into $N_E^V - 2$ triangles $\{T_i\}_{i=1}^{N_E^V-2}$ without extra vertices or edges. The $N_E^V - 3$ inner edges e_j^o (for $j = 1, \dots, N_E^V - 3$) have fixed normal \mathbf{n}_j^0 . The above notations are illustrated in Fig. 3.2.

A local space \mathcal{A}_E [41] as

$$\mathcal{A}_E = \{\mathbf{v} \in \mathbf{H}(\text{div}, E) : \mathbf{v}|_{T_i} \in \text{RT}_0(T_i), \nabla \cdot \mathbf{v} \in P_0(E) \quad \forall T_i \in E\},$$

where $\text{RT}_0(T_i)$ denotes the usual lowest-order Raviart-Thomas finite element space in simplex T_i . Naturally, the global space \mathcal{A}_h is defined as

$$\mathcal{A}_h = \{\mathbf{v} \in \mathbf{H}(\text{div}, \Omega) : \mathbf{v}|_E \in \mathcal{R}_E \quad \forall E \in \Omega_h\}.$$

Then we define the divergence-preserving reconstruction operator $\mathcal{R}_h : \mathbf{V} \rightarrow \mathcal{A}_h$ that satisfies a set of conditions as follows

$$(3.8a) \quad \int_{e_i^\partial} \mathcal{R}_h \mathbf{v} \cdot \mathbf{n}_i^\partial \, ds = \int_{e_i^\partial} \mathbf{v} \cdot \mathbf{n}_i^\partial \, ds \quad \forall \text{ boundary edge } e_i^\partial \in \partial E,$$

$$(3.8b) \quad \int_{e_i^0} [\mathcal{R}_h \mathbf{v}] \cdot \mathbf{n}_i^0 \, ds = 0 \quad \forall \text{ inner edge } e_i^0 \in E,$$

$$(3.8c) \quad \int_{T_1} \nabla \cdot (\mathcal{R}_h \mathbf{v}|_{T_i} - \mathcal{R}_h \mathbf{v}|_{T_1}) \, d\mathbf{x} = 0 \quad \text{for } i = 2, \dots, N_E^V - 2.$$

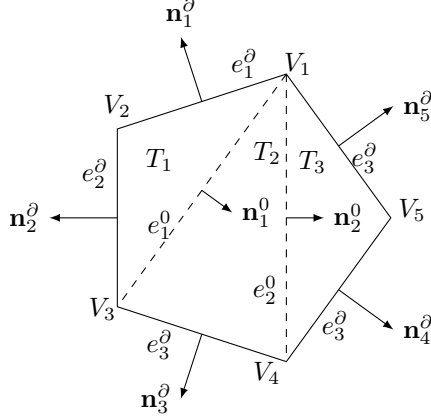


Fig. 3.2: A subtriangulation of a pentagon E and the corresponding notations.

In (3.8b), the notation $[\cdot]$ denote the jump of function on an edge. It should be emphasized that the reconstruction operator \mathcal{R}_h is explicitly computable only rely on the basis function of the lowest-order Raviart-Thomas element and degrees of freedom (3.1) of virtual element. One can see the Appendix of [41] for the implementation details of the reconstruction operator on a polygon.

The reconstruction operator \mathcal{R}_h satisfies the following properties [41, 45].

LEMMA 3.1. *For all $\mathbf{v} \in \mathbf{V}$, the reconstruction operator has the following properties*

$$(3.9a) \quad \int_e \mathcal{R}_h \mathbf{v} \cdot \mathbf{n} \, ds = \int_e \mathbf{v} \cdot \mathbf{n} \, ds \quad \forall \text{ edge } e \text{ of } E,$$

$$(3.9b) \quad \int_E \nabla \cdot \mathcal{R}_h \mathbf{v} \, dx = \int_E \nabla \cdot \mathbf{v} \, dx \quad \forall E \in \Omega_h,$$

$$(3.9c) \quad \|\mathcal{R}_h \mathbf{v} - \mathbf{v}\| \leq C_{\mathcal{R}_1} h |\mathbf{v}|_1,$$

where $C_{\mathcal{R}_1}$ is a positive constant independent of h .

Moreover, we can derive the follow result from (3.9c) and inverse inequality in [11]:

$$(3.10) \quad |\mathcal{R}_h \mathbf{v} - \mathbf{v}|_1 \leq C_{\mathcal{R}_2} |\mathbf{v}|_1,$$

where $C_{\mathcal{R}_2}$ is a positive constant independent of h .

3.3. Discrete scheme. For all $\mathbf{w}_h, \mathbf{v}_h \in \mathbf{V}_E$, we first define the computable local discrete linear form by

$$\begin{aligned} a_h^E(\mathbf{w}_h, \mathbf{v}_h) = & (\Pi^{0,E} \nabla \mathbf{w}_h, \Pi^{0,E} \nabla \mathbf{v}_h) + S_E^\nabla ((\mathbf{I} - \Pi^{\nabla,E}) \mathbf{w}_h, (\mathbf{I} - \Pi^{\nabla,E}) \mathbf{v}_h), \\ & + (\kappa^{-1} \Pi^{0,E} \mathbf{w}_h, \Pi^{0,E} \mathbf{v}_h) + S_E^0 ((\mathbf{I} - \Pi^{0,E}) \mathbf{w}_h, (\mathbf{I} - \Pi^{0,E}) \mathbf{v}_h), \end{aligned}$$

where the symmetric stabilizing bilinear forms $S_E^\nabla(\cdot, \cdot)$ and $S_E^0(\cdot, \cdot)$ satisfies

$$(3.11a) \quad C_1^\nabla \|\nabla \mathbf{v}_h\|_E^2 \leq S_E^\nabla(\mathbf{v}_h, \mathbf{v}_h) \leq C_2^\nabla \|\nabla \mathbf{v}_h\|_E^2 \quad \forall \mathbf{v}_h \in \mathbf{V}_E \text{ and } \Pi_E^\nabla \mathbf{v}_h = 0,$$

$$(3.11b) \quad C_1^0 \|\kappa^{-1/2} \mathbf{v}_h\|_E^2 \leq S_E^0(\mathbf{v}_h, \mathbf{v}_h) \leq C_2^0 \|\kappa^{-1/2} \mathbf{v}_h\|_E^2 \quad \forall \mathbf{v}_h \in \mathbf{V}_E \text{ and } \Pi_E^0 \mathbf{v}_h = 0,$$

for some positive constants $C_1^\nabla, C_2^\nabla, C_1^0$ and C_2^0 independent of h_E . Furthermore, one can easily verify $a_h^E(\cdot, \cdot)$ satisfies the consistency and the stability properties

$$(3.12a) \quad a_h^E(\mathbf{q}, \mathbf{v}_h) = a^E(\mathbf{q}, \mathbf{v}_h) \quad \forall \mathbf{q} \in [\mathbb{P}_1(E)]^2, \mathbf{v}_h \in \mathbf{V}_h,$$

$$(3.12b) \quad \alpha_* a^E(\mathbf{v}_h, \mathbf{v}_h) \leq a_h^E(\mathbf{v}_h, \mathbf{v}_h) \leq \alpha^* a^E(\mathbf{v}_h, \mathbf{v}_h) \quad \forall \mathbf{v}_h \in \mathbf{V}_h,$$

where two positive constants $\alpha_* := \min\{1, C_1^\nabla, C_1^0\}$ and $\alpha^* := \max\{1, C_2^\nabla, C_2^0\}$ are independent of h_E .

Naturally, a_h is a global extension of a_E , i.e.,

$$a_h(\mathbf{w}_h, \mathbf{v}_h) = \sum_{E \in \Omega_h} a_h^E(\mathbf{w}_h, \mathbf{v}_h) \quad \forall \mathbf{w}_h, \mathbf{v}_h \in \mathbf{V}_h.$$

The coercivity and continuity of $a_h(\cdot, \cdot)$ can be immediately obtained by the equivalent properties (3.11), Cauchy-Schwartz inequality and the definition of energy norm $\|\cdot\|$ in (2.1), i.e., there exists two positive constant C^* and $C_*(= \alpha_*)$ such that

$$(3.13a) \quad a_h(\mathbf{w}_h, \mathbf{v}_h) \leq C^* \|\mathbf{w}_h\| \|\mathbf{v}_h\| \quad \forall \mathbf{w}_h, \mathbf{v}_h \in \mathbf{V}_h,$$

$$(3.13b) \quad a_h(\mathbf{v}_h, \mathbf{v}_h) \geq C_* \|\mathbf{v}_h\|^2 \quad \forall \mathbf{v}_h \in \mathbf{V}_h.$$

Following the same approach of Lemma 4.3 in [4], the discrete inf-sup condition for the bilinear form $d(\cdot, \cdot)$ holds true, i.e., \exists constant $\tilde{\gamma} > 0$ such that

$$(3.14) \quad \sup_{\mathbf{v}_h \in \mathbf{V}_h \setminus \{\mathbf{0}\}} \frac{d(\mathbf{v}_h, q_h)}{\|\mathbf{v}_h\|} \geq \tilde{\gamma} \|q_h\| \quad \forall q_h \in Q_h.$$

Moreover, utilizing the projection property (3.9c) and Friedrichs inequality (2.2), we can deduce that for any $\mathbf{v}_h \in \mathbf{V}_h$, the following holds:

$$(3.15) \quad \begin{aligned} \|\mathcal{R}_h \mathbf{v}_h\| &= \|(\mathcal{R}_h \mathbf{v}_h - \mathbf{v}_h + \mathbf{v}_h)\| \leq (C_{\mathcal{R}_1} h + 1) \|\mathbf{v}_h\|_1 \\ &\leq C_F (C_{\mathcal{R}_1} h + 1) \|\nabla \mathbf{v}_h\| \\ &\leq \gamma^* \|\nabla \mathbf{v}_h\|, \end{aligned}$$

where we have used the boundedness of the mesh size at the last step, therefore, γ^* is a positive constant independent of κ and h .

Then we construct a really pressure-robust virtual element scheme for Brinkman problem (1.1): Find $(\mathbf{u}_h, p_h) \in \mathbf{V}_h \times Q_h$

$$(3.16a) \quad \nu a_h(\mathbf{u}_h, \mathbf{v}_h) + b(\mathbf{v}_h, p_h) = (\mathbf{f}, \mathcal{R}_h \mathbf{v}_h) \quad \forall \mathbf{v}_h \in \mathbf{V}_h,$$

$$(3.16b) \quad b(\mathbf{u}_h, q_h) = 0 \quad \forall q_h \in Q_h.$$

Combining the properties (3.13)-(3.14), one can get an immediate consequence that there exists a unique solution $(\mathbf{u}_h, p_h) \in \mathbf{V}_h \times Q_h$ of scheme (3.16). Moreover, since $\nabla \cdot \mathbf{V}_h \subset Q_h$, we can easily deduce that $\nabla \cdot \mathbf{u}_h = 0$ from (3.16b), which indicates that the scheme (3.16) is exactly divergence-free, ensuring the mass conservation of the system. Furthermore, by utilizing the discrete kernel space \mathbf{Z}_h defined in (3.7), the problem (3.16) can be formulated into the equivalent kernel form:

$$(3.17) \quad \nu a_h(\mathbf{u}_h, \mathbf{v}_h) = (\mathbb{P}(\mathbf{f}), \mathcal{R}_h \mathbf{v}_h) \quad \forall \mathbf{v}_h \in \mathbf{Z}_h,$$

where we have used the fact that $\nabla \cdot \mathcal{R}_h \mathbf{v}_h = 0$ for any $\mathbf{v} \in \mathbf{Z}_h$ from (3.9b) and the Helmholtz decomposition (2.7). Moreover, we define the notations $(\Pi^{0,h} \cdot)|_E := \Pi^{0,E} \cdot$ and $(\Pi^{\nabla,h} \cdot)|_E := \Pi^{\nabla,E} \cdot$, and give the following remark.

REMARK 3.3. Corresponding to $(\mathbf{f}, \mathcal{R}_h \mathbf{v}_h)$ in the scheme (3.16), the right-hand side term in the standard VEM scheme is constructed as $(\mathbf{f}, \Pi^{0,h} \mathbf{v}_h)$. As discussed in [21], the projection operator $\Pi^{0,h}$ changes the divergence, thus destroying the orthogonality between the divergence-free function and the gradient force. This leads to the occurrence of the locking phenomenon as $\nu \rightarrow 0$. Fortunately, we have constructed a divergence-preserving reconstruction operator \mathcal{R}_h such that $\nabla \cdot \mathcal{R}_h \mathbf{v}_h = 0$ for any $\mathbf{v}_h \in \mathbf{Z}_h$. Thus we call (3.16) as a really pressure-robust virtual element scheme, and the fact will also be proved that prior error estimate of velocity is independent of continue pressure p and viscosity ν in subsequent analysis.

Similar to (2.9), we choosing $\mathbf{v}_h = \mathbf{u}$ from (3.17), recalling the coercivity property (3.13b) and (3.15), one can deduce the

$$\begin{aligned} \nu C_* \|\mathbf{u}_h\|^2 &\leq \nu a_h(\mathbf{u}_h, \mathbf{u}_h) \leq \|\mathbb{P}(\mathbf{f})\| \cdot \|\mathcal{R}_h \mathbf{u}_h\| \\ &\leq \gamma^* \|\mathbb{P}(\mathbf{f})\| \cdot \|\nabla \mathbf{u}_h\| \\ &\leq \gamma^* \|\mathbb{P}(\mathbf{f})\| \cdot \|\mathbf{u}_h\|. \end{aligned}$$

After eliminating $\|\mathbf{u}_h\|$ from both sides, one can immediately deduce the upper bound for the velocity \mathbf{u}_h :

$$(3.18) \quad \|\mathbf{u}_h\| \leq \frac{\gamma^*}{\nu C_*} \|\mathbb{P}(\mathbf{f})\|.$$

4. A priori error analysis. In this section, we derive the optimal error estimates for the velocity error in the energy norm and the pressure error in the L^2 norm. Firstly, we provide the following classical interpolation estimates holds for the spaces \mathbf{V}_h and Q_h .

LEMMA 4.1. Let $(\mathbf{v}, p) \in ([H^2(\Omega)]^2 \cap \mathbf{V}) \times (H^1(\Omega) \cap Q)$. Then there exists an approximation $(\mathbf{v}_I, p_I) \in \mathbf{V}_h \times Q_h$ such that

$$\begin{aligned} \|\mathbf{v} - \mathbf{v}_I\| + h |\mathbf{v} - \mathbf{v}_I|_1 &\leq C_{I_1} h^2 \|\mathbf{v}\|_2, \\ \|p - p_I\| &\leq C_{I_2} h \|p\|_1, \end{aligned}$$

where the positive constants C_{I_1} and C_{I_2} are independent of h .

Then we state the following classical approximation result for $\mathbf{P}_k(E)$ space on local star-shaped domains:

LEMMA 4.2. Let $E \in \Omega_h$, and let two real numbers s, p with $0 \leq s \leq 1$ and $1 \leq p \leq \infty$. Then for all $\mathbf{u} \in [H^{s+1}(\Omega)]^2$, there exists a polynomial function $\mathbf{u}_\pi \in \mathbf{P}_k(E)$, such that

$$\|\mathbf{u} - \mathbf{u}_\pi\|_{L^p(E)} + h_E |\mathbf{u} - \mathbf{u}_\pi|_{W^{1,p}(E)} \leq C_\pi h_E^{s+1} |\mathbf{u}|_{W^{s+1,p}(E)},$$

where the positive constant C_π independent of h .

Based on the above preparations, the optimal a priori error estimate of the pressure-robust VEM scheme (3.16) is given by the following theorem.

THEOREM 4.1. Assume $(\mathbf{u}, p) \in ([H^2(\Omega)]^2 \cap \mathbf{V}) \times (H^1(\Omega) \cap Q)$ and the Assumption 3.1 holds, let (\mathbf{u}, p) and (\mathbf{u}_h, p_h) is solutions of the continue problem (2.4) and discrete problem (3.16), respectively. Then its satisfies the priori error estimates

$$(4.1a) \quad \|\mathbf{u} - \mathbf{u}_h\| \leq \tilde{C} h,$$

$$(4.1b) \quad \|p - p_h\| \leq \tilde{C} h,$$

where the positive constant $\widehat{C} := \frac{C_{\mathcal{R}_1}}{C_*} (\|\mathbf{u}\|_2 + \|\kappa^{1/2}\mathbf{u}\|) + \left(\frac{C_{\mathcal{T}_2}}{C_*} + C_{I_1} + C_{I_1} \|\kappa^{-1/2}\|_\infty \right) \|\mathbf{u}\|_2$ is independent of h , ν and pressure p , and the $\widetilde{C} := C_{I_2} \|p\|_1 + \nu \frac{C_s}{\widetilde{\gamma}}$ independent of h .

Proof. Let $\mathbf{u}_I \in \mathbf{V}_h$ be the interpolation of \mathbf{u} and satisfy the estimate (4.1). For any $\mathbf{v}_h \in \mathbf{Z}_h$, it follows that

$$\begin{aligned} (4.2) \quad \nu a_h(\mathbf{u}_h - \mathbf{u}_I, \mathbf{v}_h) &= \nu a_h(\mathbf{u}_h, \mathbf{v}_h) - \nu a_h(\mathbf{u}_I, \mathbf{v}_h) \\ &= (\mathbf{f}, \mathcal{R}_h \mathbf{v}_h) - \nu a_h(\mathbf{u}_I, \mathbf{v}_h) \\ &= [(\mathbf{f}, \mathcal{R}_h \mathbf{v}_h) - \nu a(\mathbf{u}, \mathbf{v}_h)] + [\nu a(\mathbf{u}, \mathbf{v}_h) - \nu a_h(\mathbf{u}_I, \mathbf{v}_h)] \\ &= \mathcal{T}_1 + \mathcal{T}_2. \end{aligned}$$

Then we derive the upper bounds for \mathcal{T}_1 and \mathcal{T}_2 item by item. For \mathcal{T}_1 , it follows from (1.1a) and (3.9c) that

$$\begin{aligned} (4.3) \quad \mathcal{T}_1 &= (-\nu \Delta \mathbf{u} + \nu \kappa^{-1} \mathbf{u} + \nabla p, \mathcal{R}_h \mathbf{v}_h) - \nu a(\mathbf{u}, \mathbf{v}_h) \\ &= \nu a(\mathbf{u}, \mathcal{R}_h \mathbf{v}_h - \mathbf{v}_h) \\ &= \nu (-\Delta \mathbf{u}, \mathcal{R}_h \mathbf{v}_h - \mathbf{v}_h) + \nu (\kappa^{-1} \mathbf{u}, \mathcal{R}_h \mathbf{v}_h - \mathbf{v}_h) \\ &\leq C_{\mathcal{R}_1} \nu h \left(\|\mathbf{u}\|_2 + \|\kappa^{1/2} \mathbf{u}\| \right) |\mathbf{v}_h|_1 \\ &\leq C_{\mathcal{R}_1} \nu h \left(\|\mathbf{u}\|_2 + \|\kappa^{1/2} \mathbf{u}\| \right) \|\mathbf{v}_h\|. \end{aligned}$$

For the second term, let \mathbf{u}_π be the piecewise linear polynomial projection of \mathbf{u} . Based on the consistency property (3.12a), (2.6a), (3.13a), combining Lemma 4.1 and Lemma 4.2, we have

$$\begin{aligned} (4.4) \quad \mathcal{T}_2 &= \nu a(\mathbf{u} - \mathbf{u}_\pi, \mathbf{v}_h) + \nu a(\mathbf{u}_\pi, \mathbf{v}_h) - \nu a_h(\mathbf{u}_I, \mathbf{v}_h) \\ &= \nu a(\mathbf{u} - \mathbf{u}_\pi, \mathbf{v}_h) + \nu a_h(\mathbf{u}_\pi - \mathbf{u}_I, \mathbf{v}_h) \\ &\leq \nu (C_a \|\mathbf{u} - \mathbf{u}_\pi\| + C^* \|\mathbf{u}_\pi - \mathbf{u}_I\|) \|\mathbf{v}_h\| \\ &\leq (C_\pi C_a + C_\pi C^* + C_{I_1} C^*) \nu h \|\mathbf{u}\|_2 \left(1 + h \|\kappa^{-1/2}\|_\infty \right) \|\mathbf{v}_h\| \\ &\leq C_{\mathcal{T}_2} \nu h \|\mathbf{u}\|_2 \|\mathbf{v}_h\|, \end{aligned}$$

where we have used the boundedness of the mesh size at the last step, and the constant is defined as $C_{\mathcal{T}_2} := (C_\pi C_a + C_\pi C^* + C_{I_1} C^*) (1 + \|\kappa^{-1/2}\|_\infty)$. Collecting the above (4.2)-(4.4), taking $\mathbf{v}_h := \mathbf{u}_h - \mathbf{u}_I$ and recalling the coercivity (3.13b), ones can lead to the following bound:

$$C_* \nu \|\mathbf{u}_h - \mathbf{u}_I\| \leq C_{\mathcal{R}_1} \nu h \left(\|\mathbf{u}\|_2 + \|\kappa^{1/2} \mathbf{u}\| \right) + C_{\mathcal{T}_2} \nu h \|\mathbf{u}\|_2.$$

Eliminate the symbol ν from both sides, which yields the error estimate

$$(4.5) \quad \|\mathbf{u}_h - \mathbf{u}_I\| \leq \left[\frac{C_{\mathcal{R}_1}}{C_*} \left(\|\mathbf{u}\|_2 + \|\kappa^{1/2} \mathbf{u}\| \right) + \frac{C_{\mathcal{T}_2}}{C_*} \|\mathbf{u}\|_2 \right] h.$$

The estimate (4.5) and the application of the triangle inequality conclude

$$\begin{aligned} (4.6) \quad \|\mathbf{u} - \mathbf{u}_h\| &\leq \|\mathbf{u} - \mathbf{u}_I\| + \|\mathbf{u}_h - \mathbf{u}_I\| \\ &\leq \left[\frac{C_{\mathcal{R}_1}}{C_*} \left(\|\mathbf{u}\|_2 + \|\kappa^{1/2} \mathbf{u}\| \right) + \left(\frac{C_{\mathcal{T}_2}}{C_*} + C_{I_1} + C_{I_1} \|\kappa^{-1/2}\|_\infty \right) \|\mathbf{u}\|_2 \right] h \\ &:= \widehat{C} h. \end{aligned}$$

Next we should bound the term $\|p - p_h\|$. Let p_I be the piecewise constant projection of p with respect to Ω_h . Using (1.1a) and (3.16a), we arrive at

$$\begin{aligned}
 (p_I - p_h, \nabla \cdot \mathbf{v}_h) &= (p_I, \nabla \cdot \mathbf{v}_h) + (\mathbf{f}, \mathcal{R}_h \mathbf{v}_h) - \nu a_h(\mathbf{u}_h, \mathbf{v}_h) \\
 (4.7) \quad &= (p_I, \nabla \cdot \mathbf{v}_h) + (-\nu \mathbf{u} + \nu \kappa^{-1} \mathbf{u} + \nabla p, \mathcal{R}_h \mathbf{v}_h) - \nu a_h(\mathbf{u}_h, \mathbf{v}_h) \\
 &= (p_I, \nabla \cdot \mathbf{v}_h) - (p, \nabla \cdot \mathcal{R}_h \mathbf{v}_h) + \nu a(\mathbf{u}, \mathcal{R}_h \mathbf{v}_h) - \nu a_h(\mathbf{u}_h, \mathbf{v}_h) \\
 &:= \mathcal{S}_1 + \mathcal{S}_2.
 \end{aligned}$$

For the first term \mathcal{S}_1 , we observe that p_I represents a piecewise constant in local element E , as indicated by (3.9b) and the orthogonality of L^2 -projection, which leads to

$$(4.8) \quad \mathcal{S}_1 := (p_I, \nabla \cdot \mathbf{v}_h) - (p, \nabla \cdot \mathcal{R}_h \mathbf{v}_h) = (p_I - p, \nabla \cdot \mathcal{R}_h \mathbf{v}_h) = 0.$$

For the second term \mathcal{S}_2 , repeating the similar analysis as the velocity error estimate, we deduce that

$$\begin{aligned}
 \mathcal{S}_2 &:= \nu a(\mathbf{u}, \mathcal{R}_h \mathbf{v}_h) - \nu a_h(\mathbf{u}_h, \mathbf{v}_h) \\
 &= \nu a(\mathbf{u}, \mathcal{R}_h \mathbf{v}_h - \mathbf{v}_h) + \nu a(\mathbf{u}, \mathbf{v}_h) - \nu a_h(\mathbf{u}, \mathbf{v}_h) + \nu a_h(\mathbf{u} - \mathbf{u}_h, \mathbf{v}_h) \\
 (4.9) \quad &= \nu a(\mathbf{u}, \mathcal{R}_h \mathbf{v}_h - \mathbf{v}_h) + \nu a(\mathbf{u} - \mathbf{u}_\pi, \mathbf{v}_h) - \nu a_h(\mathbf{u} - \mathbf{u}_\pi, \mathbf{v}_h) + \nu a_h(\mathbf{u} - \mathbf{u}_h, \mathbf{v}_h) \\
 &\leq \nu \left(C_a \sqrt{C_{\mathcal{R}_1}^2 + C_{\mathcal{R}_2}^2} \|\mathbf{u}\| + (C_a + C^*) C_\pi \|\mathbf{u}\|_2 (1 + \|\kappa^{-1/2}\|_\infty) + \widehat{C} \right) h \|\mathbf{v}_h\| \\
 &:= \nu C_s h \|\mathbf{v}_h\|.
 \end{aligned}$$

Then collecting the above (4.7)-(4.9), and by using the discrete inf-sup condition (3.14), it lead to

$$(4.10) \quad \|p_I - p_h\| \leq \frac{1}{\tilde{\gamma}} \sup_{\mathbf{v}_h \in \mathbf{V}_h / \{\mathbf{0}\}} \frac{d(\mathbf{v}_h, p_I - p_h)}{\|\mathbf{v}_h\|} \leq \nu \frac{C_s}{\tilde{\gamma}} h.$$

Finally, using triangle inequality, (4.10) and Lemma 4.1, we arrive at

$$(4.11) \quad \|p - p_h\| \leq \|p - p_I\| + \|p_I - p_h\| \leq \left(C_{I_2} \|p\|_1 + \nu \frac{C_s}{\tilde{\gamma}} \right) h := \tilde{C} h.$$

The proof is completed. \square

REMARK 4.1. *The really pressure-robust virtual element is Locking-free for $\nu \rightarrow 0$, and it eliminates the pressure-dependence of the velocity approximation. From the above theorem, we can observe that the constant \widehat{C} is independent of pressure p and even of viscosity ν in (4.1a). The robustness will be demonstrated through subsequently numerical examples.*

From the above Theorem 4.1 and the definition of norm $\|\cdot\|$, we have the estimate of velocity in $[H^1(\Omega)]^2$ semi-norm.

COROLLARY 4.1. *Under the same Assumption of Theorem 4.1, the priori estimate of velocity in $[H^1(\Omega)]^2$ semi-norm as follow*

$$|\mathbf{u} - \mathbf{u}_h|_1 \leq \widehat{C} h,$$

where the positive constant \widehat{C} is independent of h , ν and pressure p .

5. A posteriori error analysis and mesh adaptivity. In the section, we present a residual-type posteriori error estimator, and prove the estimator yields globally upper and locally lower bounds for the discretization error. Finally, we proposed a strategy of mesh refinement and an adaptive algorithm for VEM approximate to Brinkman problem.

Firstly, we deduce the residual error equation. Let $(\mathbf{u}, p) \in \mathbf{V} \times Q$ and $(\mathbf{u}_h, p_h) \in \mathbf{V}_h \times Q_h$ be the solutions of (2.4) and (3.16), respectively. we denote the error as

$$e_{\mathbf{u}} := \mathbf{u} - \mathbf{u}_h, \quad e_p := p - p_h.$$

Then we can obtain the error equation :

$$\begin{aligned} (5.1) \quad & \nu a(e_{\mathbf{u}}, \mathbf{v}) + b(\mathbf{v}, e_p) = (\mathbf{f}, \mathbf{v}) - \nu a(\mathbf{u}_h, \mathbf{v}) - b(\mathbf{v}, p_h) \\ & = (\mathbf{f}, \mathbf{v}) - (\mathbf{f}, \mathcal{R}_h \mathbf{v}_h) - \nu a(\mathbf{u}_h, \mathbf{v}) - b(\mathbf{v}, p_h) + \nu a_h(\mathbf{u}_h, \mathbf{v}_h) + b(\mathbf{v}_h, p_h) \\ & = (\mathbf{f}, \mathbf{v}_h - \mathcal{R}_h \mathbf{v}_h) + \nu a_h(\mathbf{u}_h, \mathbf{v}_h) - \nu a(\mathbf{u}_h, \mathbf{v}_h) - \nu a(\mathbf{u}_h, \mathbf{v} - \mathbf{v}_h) - b(\mathbf{v} - \mathbf{v}_h, p_h) + (\mathbf{f}, \mathbf{v} - \mathbf{v}_h), \end{aligned}$$

where for the last three terms, it follows from the integration by parts that

$$\begin{aligned} (5.2) \quad & -\nu a(\mathbf{u}_h, \mathbf{v} - \mathbf{v}_h) - b(\mathbf{v} - \mathbf{v}_h, p_h) + (\mathbf{f}, \mathbf{v} - \mathbf{v}_h) \\ & = -\nu (\nabla \Pi^{\nabla, h} \mathbf{u}_h, \nabla (\mathbf{v} - \mathbf{v}_h)) - \nu (\nabla (\mathbf{u}_h - \Pi^{\nabla, h} \mathbf{u}_h), \nabla (\mathbf{v} - \mathbf{v}_h)) - \nu (\kappa^{-1} \Pi^{0, h} \mathbf{u}_h, \mathbf{v} - \mathbf{v}_h) \\ & \quad - \nu (\kappa^{-1} (\mathbf{u}_h - \Pi^{0, h} \mathbf{u}_h), \mathbf{v} - \mathbf{v}_h) + (p_h, \nabla \cdot (\mathbf{v} - \mathbf{v}_h)) + (\mathbf{f}, \mathbf{v} - \mathbf{v}_h) \\ & = -\nu (\nabla (\mathbf{u}_h - \Pi^{\nabla, h} \mathbf{u}_h), \nabla (\mathbf{v} - \mathbf{v}_h)) - \nu (\kappa^{-1} (\mathbf{u}_h - \Pi^{0, h} \mathbf{u}_h), \mathbf{v} - \mathbf{v}_h) \\ & \quad + (-\nu \kappa^{-1} \Pi^{0, h} \mathbf{u}_h + \mathbf{f}, \mathbf{v} - \mathbf{v}_h) - \sum_{E \in \Omega_h} \sum_{e \in \mathcal{F}_h^0 \cap \partial E} ([\nu \nabla \Pi^{\nabla, E} \mathbf{u}_h - p_h \mathbf{I}] \mathbf{n}_e, \mathbf{v} - \mathbf{v}_h), \end{aligned}$$

where $\Delta \Pi^{\nabla, E} \mathbf{u}_h = \mathbf{0}$ and $\nabla p_h = \mathbf{0}$, due to $\Pi^{\nabla, E} \mathbf{u}_h \in \mathbf{P}_1(E)$ and p_h belonging to the set of piecewise $P_0(E)$ (denoted as Q_h). Furthermore, we can derive the final form of error equation (5.1) as follows:

$$\begin{aligned} (5.3) \quad & \nu a(e_{\mathbf{u}}, \mathbf{v}) + b(\mathbf{v}, e_p) \\ & = (\mathbf{f}, \mathbf{v}_h - \mathcal{R}_h \mathbf{v}_h) + \nu a_h(\mathbf{u}_h, \mathbf{v}_h) - \nu a(\mathbf{u}_h, \mathbf{v}_h) \\ & \quad - \nu \sum_{E \in \Omega_h} (\nabla (\mathbf{u}_h - \Pi^{\nabla, E} \mathbf{u}_h), \nabla (\mathbf{v} - \mathbf{v}_h))_E - \nu \sum_{E \in \Omega_h} (\kappa^{-1} (\mathbf{u}_h - \Pi^{0, E} \mathbf{u}_h), \mathbf{v} - \mathbf{v}_h)_E \\ & \quad + \sum_{E \in \Omega_h} (-\nu \kappa^{-1} \Pi^{0, E} \mathbf{u}_h + \mathbf{f}, \mathbf{v} - \mathbf{v}_h)_E - \sum_{E \in \Omega_h} \sum_{e \in \mathcal{F}_h^0 \cap \partial E} ([\nu \nabla \Pi^{\nabla, E} \mathbf{u}_h - p_h \mathbf{I}] \mathbf{n}_e, \mathbf{v} - \mathbf{v}_h)_e \\ & := \sum_{i=1}^5 \mathcal{J}_i. \end{aligned}$$

Inspired by [38, 42], we construct the local estimator η_E based on (5.3) as follows

$$(5.4) \quad \eta_E^2 := \eta_{\mathbf{f}, E}^2 + \eta_{S, E}^2 + \eta_{r, E}^2,$$

where

$$(5.5a) \quad \eta_{\mathbf{f}, E}^2 := h_E^2 \|\mathbf{f}\|_E^2,$$

$$(5.5b) \quad \eta_{S, E}^2 := \nu^2 S_E^{\nabla} ((I - \Pi^{\nabla, E}) \mathbf{u}_h, (I - \Pi^{\nabla, E}) \mathbf{u}_h) + \nu^2 S_E^0 ((I - \Pi^{0, E}) \mathbf{u}_h, (I - \Pi^{0, E}) \mathbf{u}_h),$$

$$(5.5c) \quad \eta_{r, E}^2 := \nu^2 h_E^2 \|\kappa^{-1} \Pi^{0, E} \mathbf{u}_h\|_E^2 + \frac{1}{2} \sum_{e \in \mathcal{F}_h^0 \cap \partial E} h_e \|[\nu \nabla \Pi^{\nabla, E} \mathbf{u}_h - p_h \mathbf{I}] \mathbf{n}_e\|_e^2.$$

The global error estimator η is defined as

$$\eta^2 = \sum_{E \in \Omega_h} \eta_E^2.$$

Before analyzing the posteriori error, we present an local interpolation result [10, 20].

LEMMA 5.1. *Under Assumption 3.1, for $\mathbf{v} \in [H^1(\Omega)]^2$, there exists a interpolation function $\mathbf{v}_I \in \mathbf{V}_h$, such that for all elements $E \in \Omega_h$, it holds that*

$$(5.6) \quad \|\mathbf{v} - \mathbf{v}_I\|_E + h_E |\mathbf{v} - \mathbf{v}_I|_{1,E} \leq \tilde{C}_I h_E |\mathbf{v}|_{1,\tilde{E}},$$

where \tilde{E} denotes the union of the polygons in Ω_h intersecting E , and the positive constant \tilde{C}_I depend only on the mesh regularity.

5.1. Upper bound. In this subsection, we will provide a global upper bound for the discretization error $\nu \|\mathbf{u} - \mathbf{u}_h\| + \|p - p_h\|$, based on the error equation (5.3).

THEOREM 5.1. *(Reliability). Let $(\mathbf{u}, p) \in \mathbf{V} \times Q$ and $(\mathbf{u}_h, p_h) \in \mathbf{V}_h \times Q_h$ be the solutions of (2.4) and (3.16), respectively. Then we can derive the following upper bound*

$$(5.7) \quad \nu \|\mathbf{u} - \mathbf{u}_h\| + \|p - p_h\| \leq C_\eta \eta,$$

where the positive constant $C_\eta := C_{\eta,u} + C_{\eta,p}$ is independent of h .

Proof. Let $e_{\mathbf{u},I} \in \mathbf{V}_h$ be the interpolation of $e_{\mathbf{u}}$ satisfying the Lemma (4.1). Taking $\mathbf{v} = e_{\mathbf{u}}$, $\mathbf{v}_h = e_{\mathbf{u},I}$ in (5.3), we now estimate \mathcal{J}_i term by term. For the first term \mathcal{J}_1 , by using (3.9c) and (5.6), it follows that

$$(5.8) \quad \begin{aligned} \mathcal{J}_1 &\leq C_{\mathcal{R}_1} h \|\mathbf{f}\| |e_{\mathbf{u},I}|_1 \leq C_{\mathcal{R}_1} h \|\mathbf{f}\| (|e_{\mathbf{u},I} - e_{\mathbf{u}}|_1 + |e_{\mathbf{u}}|_1) \\ &\leq C_{\mathcal{R}_1} h \|\mathbf{f}\| \left(\tilde{C}_I C_{\tilde{E}} |e_{\mathbf{u}}|_1 + |e_{\mathbf{u}}|_1 \right) \\ &\leq C_{\mathcal{R}_1} \left(\tilde{C}_I C_{\tilde{E}} + 1 \right) h \|\mathbf{f}\| |e_{\mathbf{u}}|_1 \\ &:= C_{\mathcal{J}_1} h \|\mathbf{f}\| \|e_{\mathbf{u}}\|, \end{aligned}$$

where the $C_{\tilde{E}}$ denotes a positive constant depending only on the mesh regularity.

For the second term \mathcal{J}_2 , a use of Lemma 4.2 and the properties (3.11) of the stabilizing terms S_E^∇

and S_E^0 yield to

$$\begin{aligned}
(5.9) \quad & \mathcal{J}_2 := \nu a_h(\mathbf{u}_h, e_{\mathbf{u},I}) - \nu a(\mathbf{u}_h, e_{\mathbf{u},I}) \\
& = -\nu (\nabla(\mathbf{u}_h - \Pi^{\nabla,h}\mathbf{u}_h), \nabla(e_{\mathbf{u},I} - \Pi^{\nabla,h}e_{\mathbf{u},I})) - \nu (\kappa^{-1}(I - \Pi^{0,h})\mathbf{u}_h, (I - \Pi^{0,h})e_{\mathbf{u},I}) \\
& \quad + \nu \sum_{E \in \Omega_h} S_E^\nabla ((I - \Pi^{\nabla,E})\mathbf{u}_h, (I - \Pi^{\nabla,E})e_{\mathbf{u},I}) + S_E^0 ((I - \Pi^{0,E})\mathbf{u}_h, (I - \Pi^{0,E})e_{\mathbf{u},I}) \\
& \leq \nu(1 + C_2^\nabla) \|\nabla(\mathbf{u}_h - \Pi^{\nabla,h}\mathbf{u}_h)\| \|\nabla(e_{\mathbf{u},I} - \Pi^{\nabla,h}e_{\mathbf{u},I})\| \\
& \quad + \nu(1 + C_2^0) \|\kappa^{-1/2}(\mathbf{u}_h - \Pi^{0,h}\mathbf{u}_h)\| \|\kappa^{-1/2}(e_{\mathbf{u},I} - \Pi^{0,h}e_{\mathbf{u},I})\| \\
& \leq \nu \frac{(1 + C_2^\nabla)C_\pi}{(C_1^\nabla)^{1/2}} \sum_{E \in \Omega_h} (S_E^\nabla((I - \Pi^{\nabla,E})\mathbf{u}_h, (I - \Pi^{\nabla,E})\mathbf{u}_h))^{1/2} |e_{\mathbf{u},I}|_1 \\
& \quad + \nu \frac{(1 + C_2^0)C_\pi}{(C_1^0)^{1/2}} h \sum_{E \in \Omega_h} (S_E^0((I - \Pi^{0,E})\mathbf{u}_h, (I - \Pi^{0,E})\mathbf{u}_h))^{1/2} \|\kappa^{-1/2}\|_\infty |e_{\mathbf{u},I}|_1 \\
& \leq \nu C_{\mathcal{J}_2} \|\mathbf{e}_\mathbf{u}\| \sum_{E \in \Omega_h} (S_E^\nabla((I - \Pi^{\nabla,E})\mathbf{u}_h, (I - \Pi^{\nabla,E})\mathbf{u}_h))^{1/2} + (S_E^0((I - \Pi^{0,E})\mathbf{u}_h, (I - \Pi^{0,E})\mathbf{u}_h))^{1/2},
\end{aligned}$$

where the positive constant $C_{\mathcal{J}_2} := (\tilde{C}_I C_{\tilde{E}} + 1) \max \left\{ \frac{(1 + C_2^\nabla)C_\pi}{(C_1^\nabla)^{1/2}}, \frac{(1 + C_2^0)C_\pi}{(C_1^0)^{1/2}} \|\kappa^{-1/2}\|_\infty \right\}$ is a positive constant independent of h , and the same trick as used in (5.8) is employed in last step.

Similar to the proof of \mathcal{J}_2 , one can derive the bound of \mathcal{J}_3 as follows

$$(5.10) \quad \mathcal{J}_3 \leq \nu C_{\mathcal{J}_3} \|\mathbf{e}_\mathbf{u}\| \sum_{E \in \Omega_h} (S_E^\nabla((I - \Pi^{\nabla,E})\mathbf{u}_h, (I - \Pi^{\nabla,E})\mathbf{u}_h))^{1/2} + (S_E^0((I - \Pi^{0,E})\mathbf{u}_h, (I - \Pi^{0,E})\mathbf{u}_h))^{1/2},$$

where the positive constant $C_{\mathcal{J}_3} := \tilde{C}_I C_{\tilde{E}} \max \left\{ \frac{1}{(C_1^\nabla)^{1/2}}, \frac{\|\kappa^{-1/2}\|_\infty}{(C_1^0)^{1/2}} \right\}$ is a positive constant independent of h .

The estimate of \mathcal{J}_4 also can be easily carried out

$$\begin{aligned}
(5.11) \quad & \mathcal{J}_4 := \sum_{E \in \Omega_h} (-\nu \kappa^{-1} \Pi^{0,E} \mathbf{u}_h + \mathbf{f}, e_{\mathbf{u}} - e_{\mathbf{u},I})_E \\
& \leq \| -\nu \kappa^{-1} \Pi^{0,h} \mathbf{u}_h + \mathbf{f} \| \| e_{\mathbf{u}} - e_{\mathbf{u},I} \| \\
& \leq \tilde{C}_I C_{\tilde{E}} h \| -\nu \kappa^{-1} \Pi^{0,h} \mathbf{u}_h + \mathbf{f} \| \| e_{\mathbf{u}} \| \\
& := C_{\mathcal{J}_4} h (\nu \| \kappa^{-1} \Pi^{0,h} \mathbf{u}_h \| + \| \mathbf{f} \|) \| e_{\mathbf{u}} \|.
\end{aligned}$$

Before estimating \mathcal{J}_5 , we use Young's inequality to give a variant of the trace inequality: $\exists C_{\text{tra}}$ that is independent of h_E such that

$$\|w\|_e \leq \frac{\sqrt{2}C_{\text{tra}}}{2} (h_E^{-1} \|w\|_E^2 + h_E |w|_{1,E}^2)^{1/2} \quad \text{for any edge } e \in \partial E.$$

Finally, by using Cauchy-Schwartz inequality, trace inequality and Lemma 5.1, we arrive at the bound of

the last term \mathcal{J}_5 as follows

$$\begin{aligned}
\mathcal{J}_5 &\leq \sum_{E \in \Omega_h} \sum_{e \in \mathcal{F}_h^0 \cap \partial E} \|[\nu \nabla \Pi^{\nabla, E} \mathbf{u}_h - p_h \mathbf{I}] \mathbf{n}_e\|_e \|e_{\mathbf{u}} - e_{\mathbf{u}, I}\|_e \\
&\leq \left(\sum_{E \in \Omega_h} \sum_{e \in \mathcal{F}_h^0 \cap \partial E} \|[\nu \nabla \Pi^{\nabla, E} \mathbf{u}_h - p_h \mathbf{I}] \mathbf{n}_e\|_e^2 \right)^{1/2} \left(\sum_{E \in \Omega_h} \sum_{e \in \mathcal{F}_h^0 \cap \partial E} \|e_{\mathbf{u}} - e_{\mathbf{u}, I}\|_e^2 \right)^{1/2} \\
&\leq \frac{\sqrt{2} C_{\text{tra}}}{2} \left(\sum_{E \in \Omega_h} \sum_{e \in \mathcal{F}_h^0 \cap \partial E} \|[\nu \nabla \Pi^{\nabla, E} \mathbf{u}_h - p_h \mathbf{I}] \mathbf{n}_e\|_e^2 \right)^{1/2} \left(\sum_{E \in \Omega_h} h_E^{-1} \|e_{\mathbf{u}} - e_{\mathbf{u}, I}\|_E^2 + h_E |e_{\mathbf{u}} - e_{\mathbf{u}, I}|_{1, E}^2 \right)^{1/2} \\
&\leq C_{\text{tra}} \tilde{C}_I \left(\sum_{E \in \Omega_h} \sum_{e \in \mathcal{F}_h^0 \cap \partial E} \|[\nu \nabla \Pi^{\nabla, E} \mathbf{u}_h - p_h \mathbf{I}] \mathbf{n}_e\|_e^2 \right)^{1/2} \left(\sum_{E \in \Omega_h} h_E |e_{\mathbf{u}}|_{1, \tilde{E}}^2 \right)^{1/2}.
\end{aligned}$$

Recalling the Assumption 3.1, we arrive at

$$\begin{aligned}
(5.12) \quad \mathcal{J}_5 &\leq \frac{\sqrt{2} C_{\text{tra}} \tilde{C}_I C_{\tilde{E}}}{\sqrt{\rho}} \left(\frac{1}{2} \sum_{E \in \Omega_h} \sum_{e \in \mathcal{F}_h^0 \cap \partial E} h_e \|[\nu \nabla \Pi^{\nabla, E} \mathbf{u}_h - p_h \mathbf{I}] \mathbf{n}_e\|_e^2 \right)^{1/2} \|\mathbf{e}_{\mathbf{u}}\| \\
&:= C_{\mathcal{J}_5} \left(\frac{1}{2} \sum_{E \in \Omega_h} \sum_{e \in \mathcal{F}_h^0 \cap \partial E} h_e \|[\nu \nabla \Pi^{\nabla, E} \mathbf{u}_h - p_h \mathbf{I}] \mathbf{n}_e\|_e^2 \right)^{1/2} \|\mathbf{e}_{\mathbf{u}}\|.
\end{aligned}$$

Since $\nabla \cdot \mathbf{u}_h = 0$ and (2.4b), then $b(\mathbf{e}_{\mathbf{u}}, e_p) = 0$. Thus, combining (5.8)-(5.12) to (5.3), we deduce that

$$(5.13) \quad \nu \|\mathbf{u} - \mathbf{u}_h\| \leq C_{\eta, u} \eta,$$

where the positive constant $C_{\eta, u} := \max \{C_{\mathcal{J}_1} + C_{\mathcal{J}_4}, 2(C_{\mathcal{J}_2} + C_{\mathcal{J}_3}), 2(C_{\mathcal{J}_4} + C_{\mathcal{J}_5})\}$.

To end the proof, we remain to estimate the error for the pressure. It follows from the (2.4a) and (3.16a), the orthogonality of $\Pi^{\nabla, E}$ and $\Pi^{0, E}$ that

$$\begin{aligned}
(5.14) \quad (\nabla \cdot \mathbf{v}, p - p_h) &= b(\mathbf{v}, p) - b(\mathbf{v}, p_h) \\
&= (\mathbf{f}, \mathbf{v}) - \nu a(\mathbf{u}, \mathbf{v}) - (\nabla \cdot (\mathbf{v} - \mathbf{v}_I), p_h) - (\nabla \cdot \mathbf{v}_I, p_h) \\
&= -\nu a(\mathbf{u}, \mathbf{v}) + \nu a_h(\mathbf{u}_h, \mathbf{v}_I) + (\mathbf{f}, \mathbf{v}) - (\mathbf{f}, \mathcal{R}_h \mathbf{v}_I) - (\nabla \cdot (\mathbf{v} - \mathbf{v}_I), p_h) \\
&= -\nu (\nabla \mathbf{u} - \nabla \Pi^{\nabla, h} \mathbf{u}_h, \nabla \mathbf{v}) - \nu (\nabla \Pi^{\nabla, h} \mathbf{u}_h, \nabla \mathbf{v} - \nabla \mathbf{v}_I + \nabla \mathbf{v}_I - \nabla \Pi^{\nabla, h} \mathbf{v}_I) \\
&\quad - \nu (\kappa^{-1}(\mathbf{u} - \Pi^{0, h} \mathbf{u}_h), \mathbf{v}) - \nu (\kappa^{-1} \Pi^{0, h} \mathbf{u}_h, \mathbf{v} - \mathbf{v}_I + \mathbf{v}_I - \Pi^{0, h} \mathbf{v}_I) \\
&\quad + \nu \sum_{E \in \Omega_h} S_E^\nabla ((I - \Pi^{\nabla, E}) \mathbf{u}_h, (I - \Pi^{\nabla, E}) \mathbf{v}_I) + S_E^0 ((I - \Pi^{0, E}) \mathbf{u}_h, (I - \Pi^{0, E}) \mathbf{v}_I) \\
&\quad - (\nabla \cdot (\mathbf{v} - \mathbf{v}_I), p_h) + (\mathbf{f}, \mathbf{v}) - (\mathbf{f}, \mathcal{R}_h \mathbf{v}_I).
\end{aligned}$$

Using the integration by parts, we derive the following error equation of pressure
(5.15)

$$\begin{aligned}
& (\nabla \cdot \mathbf{v}, p - p_h) \\
&= -\nu (\nabla(\mathbf{u} - \mathbf{u}_h + \mathbf{u}_h - \Pi^{\nabla,h} \mathbf{u}_h), \nabla \mathbf{v}) - \nu (\kappa^{-1}(\mathbf{u} - \mathbf{u}_h + \mathbf{u}_h - \Pi^{0,h} \mathbf{u}_h), \mathbf{v}) - \nu (\kappa^{-1} \Pi^{0,h} \mathbf{u}_h, \mathbf{v} - \mathbf{v}_I) \\
&\quad + \nu \sum_{E \in \Omega_h} S_E^\nabla ((I - \Pi^{\nabla,E}) \mathbf{u}_h, (I - \Pi^{\nabla,E}) \mathbf{v}_I) + S_E^0 ((I - \Pi^{0,E}) \mathbf{u}_h, (I - \Pi^{0,E}) \mathbf{v}_I) \\
&\quad + (\mathbf{f}, \mathbf{v} - \mathbf{v}_I) - (\mathbf{f}, \mathcal{R}_h \mathbf{v}_I - \mathbf{v}_I) - \sum_{E \in \Omega_h} \sum_{e \in \mathcal{F}_h^0 \cap \partial E} ([\nu \nabla \Pi^{\nabla,E} \mathbf{u}_h - p_h \mathbf{I}] \mathbf{n}_e, \mathbf{v} - \mathbf{v}_I).
\end{aligned}$$

Then similar to the proofs of (5.8)-(5.12), and combining the estimate (5.13) of velocity and the discrete inf-sup condition (3.14), one can easily derive the desired result for the pressure from error equation (5.15).

$$\|p - p_h\| \leq C_{\eta,p} \eta,$$

where the positive constant $C_{\eta,p}$ is independent of h . This concludes the proof. \square

5.2. Local Lower Bound. Before proving the local lower bound, we need to introduce a important tool called bubble function. Under the mesh regularity assumption, each element E admits a sub-triangulation by connecting each vertex of E to the point \mathbf{x}_E with respect to which E is star-shaped. Then, a bubble function $\psi_E \in [H_0^1(E)]^2$ can be constructed piecewise as the sum of the cubic bubble functions on each triangle of the sub-triangulation of E . An edge bubble function ψ_e for $e \subset \partial E$ is a piecewise quadratic function with a value of $\mathbf{1}$ at the middle point of e and $\mathbf{0}$ on the triangles that do not include e as their boundary. The bubble functions have the following properties [38, 42]

LEMMA 5.2. *On each element $E \in \Omega_h$, the bubble function ψ_E satisfies*

$$(5.16a) \quad C_{B_1} \|\mathbf{p}_1\|_E^2 \leq (\psi_E \mathbf{p}_1, \mathbf{p}_1)_E \leq C_{B_2} \|\mathbf{p}_1\|_E^2 \quad \forall \mathbf{p}_1 \in \mathbf{P}_1(E),$$

$$(5.16b) \quad C_{B_3} \|\mathbf{p}_1\|_E^2 \leq \|\psi_E \mathbf{p}_1\|_E + h_E \|\nabla(\psi_E \mathbf{p}_1)\|_E \leq C_{B_4} \|\mathbf{p}_1\|_E^2 \quad \forall \mathbf{p}_1 \in \mathbf{P}_1(E),$$

where the positive constants $C_{B_1}, C_{B_2}, C_{B_3}$ and C_{B_4} are independent of h_E . Moreover, For any $e \subset \partial E$ the edge bubble function ψ_e satisfies

$$(5.17a) \quad C_{b_1} \|\mathbf{p}_1\|_e^2 \leq (\psi_e \mathbf{p}_1, \mathbf{p}_1)_e \leq C_{b_2} \|\mathbf{p}_1\|_e^2 \quad \forall \mathbf{p}_1 \in \mathbf{P}_1(e),$$

$$(5.17b) \quad h_E^{-1/2} \|\psi_e \mathbf{p}_1\|_E + h_E^{1/2} \|\nabla(\psi_e \mathbf{p}_1)\|_E \leq C_{b_3} \|\mathbf{p}_1\|_e \quad \forall \mathbf{p}_1 \in \mathbf{P}_1(e),$$

where the positive constants $C_{b_1}, C_{b_2}, C_{b_3}$ and C_{b_4} are independent of h_E and h_e , and $\psi_e \mathbf{p}_1$ is extended from e to E by the technique introduced in Remark 3.1 of [32].

THEOREM 5.2. (Efficiency). *Let $(\mathbf{u}, p) \in \mathbf{V} \times Q$ and $(\mathbf{u}_h, p_h) \in \mathbf{V}_h \times Q_h$ be the solutions of (2.4) and (3.16), respectively. Then, the local estimator $\eta_{r,E}$ satisfy*

$$(5.18) \quad \eta_{r,E}^2 \leq C_r \sum_{E \in \mathcal{E}_e} (\nu^2 \|\mathbf{u} - \mathbf{u}_h\|_E^2 + \|p - p_h\|_E^2 + \eta_{S,E}^2 + \eta_{f,E}^2 + \nu^2 h_E^2 \|\kappa^{-1} \Pi^{0,E} \mathbf{u}_h\|_E^2),$$

where the positive constant $C_r := C_e \max\{1, C_\theta\}$ is independent of h_E .

Proof. To be simple, we use θ_E to denote the local residual $\kappa^{-1} \Pi^{0,E} \mathbf{u}_h$. We readily observe that θ_E is a vector linear polynomial on E . By using bubble function ψ_E on E , we set $\mathbf{v} = \psi_E \theta_E$ and $\mathbf{v}_h = 0$ in

(5.3), and note that ψ_E vanishes on boundary ∂E , we arrive at

$$(5.19) \quad \begin{aligned} & \nu(\nabla e_{\mathbf{u}}, \nabla \psi_E \theta_E)_E + \nu(\kappa^{-1} e_{\mathbf{u}}, \psi_E \theta_E)_E + (\nabla \cdot (\psi_E \theta_E), e_p)_E \\ &= -\nu(\nabla(\mathbf{u}_h - \Pi^{\nabla, E} \mathbf{u}_h), \nabla \psi_E \theta_E)_E - \nu(\kappa^{-1}(\mathbf{u}_h - \Pi^{0, E} \mathbf{u}_h), \psi_E \theta_E)_E + (-\nu \theta_E + \mathbf{f}, \psi_E \theta_E)_E. \end{aligned}$$

Utilizing the properties the properties (5.16) of the bubble function ψ_E , we obtain

$$\begin{aligned} C_{B_1} \nu \|\theta_E\|_E^2 &\leq \nu(\theta_E, \psi_E \theta_E) \\ &= -\nu(\nabla e_{\mathbf{u}}, \psi_E \theta_E)_E - \nu(\kappa^{-1} e_{\mathbf{u}}, \psi_E \theta_E)_E - (\nabla \cdot (\psi_E \theta_E), e_p)_E + (\mathbf{f}, \psi_E \theta_E) \\ &\quad - \nu(\nabla(\mathbf{u}_h - \Pi^{\nabla, E} \mathbf{u}_h), \nabla \psi_E \theta_E)_E - \nu(\kappa^{-1}(\mathbf{u}_h - \Pi^{0, E} \mathbf{u}_h), \psi_E \theta_E)_E \\ &\leq \nu|e_{\mathbf{u}}|_{1, E} |\psi_E \theta_E|_{1, E} + \nu \|\kappa^{-1/2}\|_{\infty} \|\kappa^{-1/2} e_{\mathbf{u}}\|_E \|\psi_E \theta_E\|_E + \|p - p_h\|_E |\psi_E \theta_E|_{1, E} \\ &\quad + \frac{\nu}{(C_1^{\nabla})^{1/2}} S_E^{\nabla}((I - \Pi^{\nabla, E}) \mathbf{u}_h, (I - \Pi^{\nabla, E}) \mathbf{u}_h)^{1/2} |\psi_E \theta_E|_{1, E} + \|\mathbf{f}\|_E \|\psi_E \theta_E\|_E \\ &\quad + \frac{\nu \|\kappa^{-1/2}\|_{\infty}}{(C_1^0)^{1/2}} S_E^0((I - \Pi^{0, E}) \mathbf{u}_h, (I - \Pi^{0, E}) \mathbf{u}_h)^{1/2} \|\psi_E \theta_E\|_E. \end{aligned}$$

Furthermore,

$$\nu \|\theta_E\|_E^2 \leq C_{\theta_1} (\nu|e_{\mathbf{u}}|_{1, E} + \|e_p\|_E + \eta_{S, E}) h_E^{-1} \|\theta_E\|_E + C_{\theta_2} \left(\nu \|\kappa^{-1/2} e_{\mathbf{u}}\|_E + \|f\|_E + \eta_{S, E} \right) \|\theta_E\|_E,$$

where the positive constants $C_{\theta_1} := \frac{C_{B_4}}{C_{B_1}} \cdot \max \left\{ 2, \frac{1}{(C_1^{\nabla})^{1/2}} \right\}$ and $C_{\theta_2} := \frac{C_{B_4}}{C_{B_1}} \cdot \max \left\{ 1, \frac{\|\kappa^{-1/2}\|_{\infty}}{(C_1^0)^{1/2}}, \|\kappa^{-1/2}\|_{\infty} \right\}$ are both independent of h_E . Then, eliminating $\|\theta_E\|_E$ and multiplying h_E on both sides give

$$(5.20) \quad \nu^2 h_E^2 \|\theta_E\|_E^2 \leq C_{\theta} (\nu^2 \|e_{\mathbf{u}}\|_E^2 + \|e_p\|_E^2 + \eta_{S, E}^2 + \eta_{\mathbf{f}, E}^2),$$

where the positive constant $C_{\theta} := 4(C_{\theta_1} + C_{\theta_2})^2$, and the boundedness of the mesh size is used.

On the other hand, we define θ_e as $[\nu \Pi^{\nabla, E} \mathbf{u}_h - p_h \mathbf{I}] \mathbf{n}_e$, and subsequently extend θ_e into \mathcal{E}_e via a constant vector prolongation in the direction normal to e (see [32], Remark 3.1). Let ψ_e represent an edge bubble function on e . By setting $\mathbf{v} = \psi_e \theta_e, \mathbf{v}_h = \mathbf{0}$ in (5.3), we derive the following result:

$$\begin{aligned} & \nu \sum_{E \in \mathcal{E}_e} (\nabla e_{\mathbf{u}}, \nabla \psi_e \theta_e)_E + \nu \sum_{E \in \mathcal{E}_e} (\kappa^{-1} e_{\mathbf{u}}, \psi_e \theta_e)_E + \sum_{E \in \mathcal{E}_e} (\nabla \cdot (\psi_e \theta_e), e_p)_E \\ &= -\nu \sum_{E \in \mathcal{E}_e} (\nabla(\mathbf{u}_h - \Pi^{\nabla, E} \mathbf{u}_h), \nabla \psi_e \theta_e)_E - \nu \sum_{E \in \mathcal{E}_e} (\kappa^{-1}(\mathbf{u}_h - \Pi^{0, E} \mathbf{u}_h), \psi_e \theta_e)_E \\ &\quad + \sum_{E \in \mathcal{E}_e} (-\nu \kappa^{-1} \Pi^{0, E} \mathbf{u}_h + \mathbf{f}, \psi_e \theta_e)_E - (\theta_e, \psi_e \theta_e)_e. \end{aligned}$$

Using the properties (5.17), we can deduce that

$$\begin{aligned} C_{b_1} \|\theta_e\|_e^2 &\leq (\theta_e, \psi_e \theta_e)_e \leq C_{e_1} \sum_{E \in \mathcal{E}_e} (\nu|e_{\mathbf{u}}|_{1, E} + \|e_p\|_E + \eta_{S, E}) |\psi_e \theta_e|_{1, E} \\ &\quad + C_{e_2} \sum_{E \in \mathcal{E}_e} \left(\nu \|\kappa^{-1/2} e_{\mathbf{u}}\|_E + \nu \|\kappa^{-1} \Pi^{0, E} \mathbf{u}_h\| + \|\mathbf{f}\|_E + \eta_{S, E} \right) \|\psi_e \theta_e\|_E \\ &\leq C_{e_1} C_{b_3} \sum_{E \in \mathcal{E}_e} h_E^{-1/2} (\nu|e_{\mathbf{u}}|_{1, E} + \|e_p\|_E + \eta_{S, E}) \|\theta_e\|_e \\ &\quad + C_{e_2} C_{b_3} \sum_{E \in \mathcal{E}_e} h_E^{1/2} \left(\nu \|\kappa^{-1/2} e_{\mathbf{u}}\|_E + \nu \|\theta_E\| + \|\mathbf{f}\|_E + \eta_{S, E} \right) \|\theta_e\|_e, \end{aligned}$$

where $C_{e_1} := \max \left\{ 2, \frac{1}{(C_1^V)^{1/2}} \right\}$ and $C_{e_2} := \max \left\{ 1, \frac{\|\kappa^{-1/2}\|}{(C_1^0)^{1/2}}, \|\kappa^{-1/2}\| \right\}$. Above, multiplying h_e on both sides yields

$$(5.21) \quad \begin{aligned} h_e \|\theta_e\|_e^2 &\leq \frac{C_{e_1} C_{b_3}}{C_{b_1}} \sum_{E \in \mathcal{E}_e} (\nu |e_{\mathbf{u}}|_{1,E} + \|e_p\|_E + \eta_{S,E}) h_e^{1/2} \|\theta_e\|_e \\ &\quad + \frac{C_{e_2} C_{b_3}}{C_{b_1}} \sum_{E \in \mathcal{E}_e} h_E \left(\nu \|\kappa^{-1/2} e_{\mathbf{u}}\|_E + \nu \|\theta_E\| + \|\mathbf{f}\|_E + \eta_{S,E} \right) h_e^{1/2} \|\theta_e\|_e. \end{aligned}$$

By cancelling $h_e^{1/2} \|\theta_e\|$, it follows that there exists a positive constant C_e , which is related to $\frac{C_{e_1} C_{b_3}}{C_{b_1}}$ and $\frac{C_{e_2} C_{b_3}}{C_{b_1}}$ and independent of h_E and h_e , such that

$$(5.22) \quad \frac{1}{2} h_e \|\theta_e\|_e^2 \leq C_e \sum_{E \in \mathcal{E}_e} (\nu^2 \|e_{\mathbf{u}}\|_E^2 + \|e_p\|_E^2 + \eta_{S,E}^2 + \eta_{\mathbf{f},E}^2 + \nu^2 h_E^2 \|\theta_E\|_E^2).$$

By summing over all edges $e \subset \partial E$ for (5.22), together with (5.20), we can deduce that

$$(5.23) \quad \eta_{r,E}^2 \leq C_r \sum_{E \in \mathcal{E}_e} (\nu^2 \|e_{\mathbf{u}}\|_E^2 + \|e_p\|_E^2 + \eta_{S,E}^2 + \eta_{\mathbf{f},E}^2 + \nu^2 h_E^2 \|\theta_E\|_E^2),$$

where $C_r := C_e \max\{1, C_\theta\}$ is independent of h_E . The proof is completed. \square

5.3. An adaptive mesh refinement. We perform refinement on the local polygon as shown in Fig. 5.1. By connecting the centroid of the heptagon with the midpoint of each edge, we obtain a set of sub-quadrilaterals. It should be noted that when there is a hanging point on an edge, in order to prevent degenerate triangles from appearing during the refinement process, we directly connect the centroid and the hanging point (rather than the midpoint of hanging point and the endpoint). Please refer to the mVEM package [46] for more details. Then we introduce a adaptive algorithm as follows:

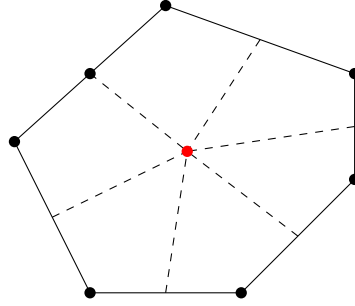


Fig. 5.1: Illustration of refining a local heptagon.

Given an initial coarse mesh Ω_h , we compute the numerical solution (\mathbf{u}_h, p_h) of (3.16), and the local estimator η_E on each element of the grid. Then, we choose a set $\mathcal{T}_h \subset \Omega_h$ with minimum number such that

$$(5.24) \quad \sum_{E \in \mathcal{T}_h} \eta_E^2 \geq \delta \sum_{E \in \Omega_h} \eta_E^2,$$

where $\delta \in (0, 1)$ is a marking parameter. We can briefly summarize this procedure with the well-known four steps:

Solve \rightarrow Estimate \rightarrow Mark \rightarrow Refine.

The loop is stopped by a user-specified iteration number \mathcal{L} , or until the number \mathcal{N} of nodes in the mesh satisfies $\mathcal{N} \geq \mathbf{tol}$, where \mathbf{tol} is the user-specified tolerance of nodal number.

6. Numerical results. In this section we present some examples illustrate the method's practical performance. As we emphasized in [44], we cannot pointwise access to the numerical solution of velocity $\mathbf{u}_h \in \mathbf{V}_h$ within the element. Consequently, we use the projections $\Pi^{\nabla, h} \mathbf{u}_h$ and $\Pi^{0, h} \mathbf{u}_h$ as a substitute for \mathbf{u}_h to calculate the error. Considering the computable error quantity

$$\left(\sum_{E \in \Omega_h} \|\nabla \mathbf{u} - \nabla \Pi^{\nabla, E} \mathbf{u}_h\|_{0, E}^2 + \left\| \kappa^{-1/2} (\mathbf{u} - \Pi^{0, E} \mathbf{u}_h) \right\|_{0, E}^2 \right)^{1/2}$$

as approximation of $\|\mathbf{u} - \mathbf{u}_h\|$. And for the error of pressures we simply compute

$$\|p - p_h\| := \left(\sum_{E \in \Omega_h} \|p - p_h\|_{0, E}^2 \right)^{1/2}.$$

Moreover, three types of polygonal meshes will be used in the following Numerical results, that is non-convex mesh, square mesh and Voronoi mesh generated by the PolyMesher [34] (see Fig. 6.1 for illustration).

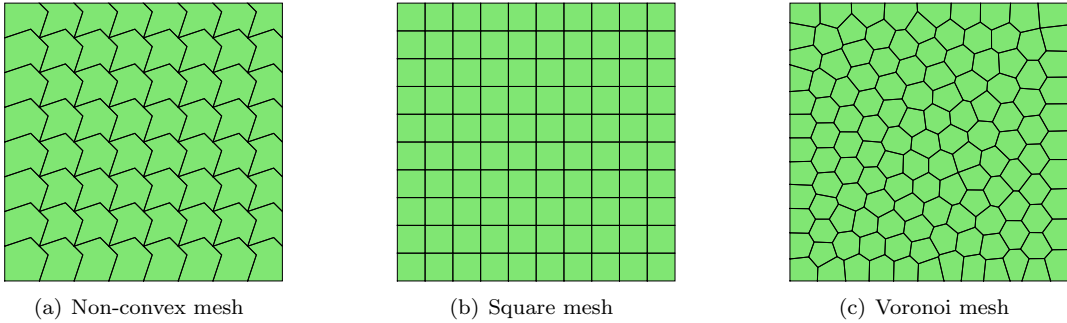


Fig. 6.1: Illustration of three types of meshes.

6.1. Numerical tests for a priori error estimate. In this subsection, three numerical experiments are investigated to validate our theorem 4.1 and numerically simulate the flow of fluids in practical problems.

EXAMPLE 6.1. Let the domain be square $\Omega = (0, 1) \times (0, 1)$, which is partitioned into non-convex mesh Fig. 6.1(a). To study the robustness of our virtual element methods to the parameter ν , we fixed $\kappa = 1$ and select different $\nu = 1, 10^{-4}, 10^{-8}, 10^{-12}$. The exact solution for (1.1) is chosen as follows :

$$(6.1) \quad \mathbf{u} = \begin{pmatrix} \sin(2\pi x) \cos(2\pi y) \\ -\cos(2\pi x) \sin(2\pi y) \end{pmatrix}, \quad p = x^2 y^2 - 1/9,$$

where the load function \mathbf{f} is suitably chosen, and it is easy to check that $\nabla \cdot \mathbf{u} = 0$ and $(p, 1) = 0$.

We show the numerical results on Table 6.1. Compared to the standard VEM scheme, our pressure-robust VEM scheme is Locking-free for viscosity $\nu \rightarrow 0$. And apparently, the error of velocity does not even change due to ν , which is consistent with what we have been discussing in remark 4.1. Our numerical results demonstrate that the pressure-robust VEM scheme is accurate and robust.

Table 6.1: Example 1: Comparison of the standard and pressure-robust virtual element scheme for $\nu = 1, 10^{-4}, 10^{-8}, 10^{-12}$ with a fixed $\kappa = 1$.

ν	h	Standard VEM			Pressure-robust VEM			
		$\ \mathbf{u} - \mathbf{u}_h\ $	Rate	$\ p - p_h\ $	Rate	$\ \mathbf{u} - \mathbf{u}_h\ $	Rate	$\ p - p_h\ $
1	1.00e-01	1.681e+00	-	1.997e-01	-	1.681e+00	-	2.328e-01
	5.00e-02	8.175e-01	1.04	7.290e-02	1.45	8.172e-01	1.04	8.049e-02
	2.50e-02	4.042e-01	1.02	3.095e-02	1.24	4.041e-01	1.02	3.216e-02
	1.25e-02	2.015e-01	1.00	1.499e-02	1.05	2.015e-01	1.00	1.497e-02
1e-4	1.00e-01	1.688e+00	-	2.157e-02	-	1.681e+00	-	2.157e-02
	5.00e-02	8.177e-01	1.05	1.106e-02	0.96	8.172e-01	1.04	1.106e-02
	2.50e-02	4.042e-01	1.02	5.034e-03	1.14	4.041e-01	1.02	5.034e-03
	1.25e-02	2.015e-01	1.00	2.655e-03	0.92	2.015e-01	1.00	2.655e-03
1e-8	1.00e-01	\times	-	2.157e-02	-	1.681e+00	-	2.157e-02
	5.00e-02	\times	-	1.106e-02	0.96	8.172e-01	1.04	1.106e-02
	2.50e-02	\times	-	5.034e-03	1.14	4.041e-01	1.02	5.034e-03
	1.25e-02	\times	-	2.655e-03	0.92	2.015e-01	1.00	2.655e-03
1e-12	1.00e-01	\times	-	2.157e-02	-	1.681e+00	-	2.157e-02
	5.00e-02	\times	-	1.106e-02	0.96	8.172e-01	1.04	1.106e-02
	2.50e-02	\times	-	5.034e-03	1.14	4.041e-01	1.02	5.034e-03
	1.25e-02	\times	-	2.655e-03	0.92	2.015e-01	1.00	2.655e-03

In the following two high contrast permeability numerical examples, a 128×128 square mesh (as shown in Fig. 6.1(b)) is used to test the robustness of our scheme with respect to the permeability κ . The following two test problems have the same data setting:

$$\Omega = (0, 1) \times (0, 1), \quad \nu = 0.01, \quad \mathbf{f} = \mathbf{0} \quad \text{and} \quad \mathbf{u} = \begin{pmatrix} 1 \\ 0 \end{pmatrix} \text{ on } \partial\Omega.$$

EXAMPLE 6.2. This example is frequently used in filtration and insulation materials. The inverse of permeability of fibrous structure is shown in Fig. 6.2(a), where $\kappa_{\min}^{-1} = 1$ and $\kappa_{\max}^{-1} = 10^6$ in the red and blue regions, respectively. The pressure profile of the pressure-robust is presented in Fig. 6.2(e). The first and the second components of the velocity calculated by our scheme are shown in Fig. 6.2(c) and 6.2(d), respectively. It is evident that the outcomes are congruent with those reported in the study by Zhai et al. [47].

EXAMPLE 6.3. The geometry of this example is an open foam with a profile of κ^{-1} shown in Fig. 6.3(a), where $\kappa_{\min}^{-1} = 1$ and $\kappa_{\max}^{-1} = 10^6$ in the red and blue regions, respectively. The profiles of the approximate pressure and velocity are presented in Fig. 6.3. It is observed that the findings are analogous to those presented in the work by Wang et al. [39].

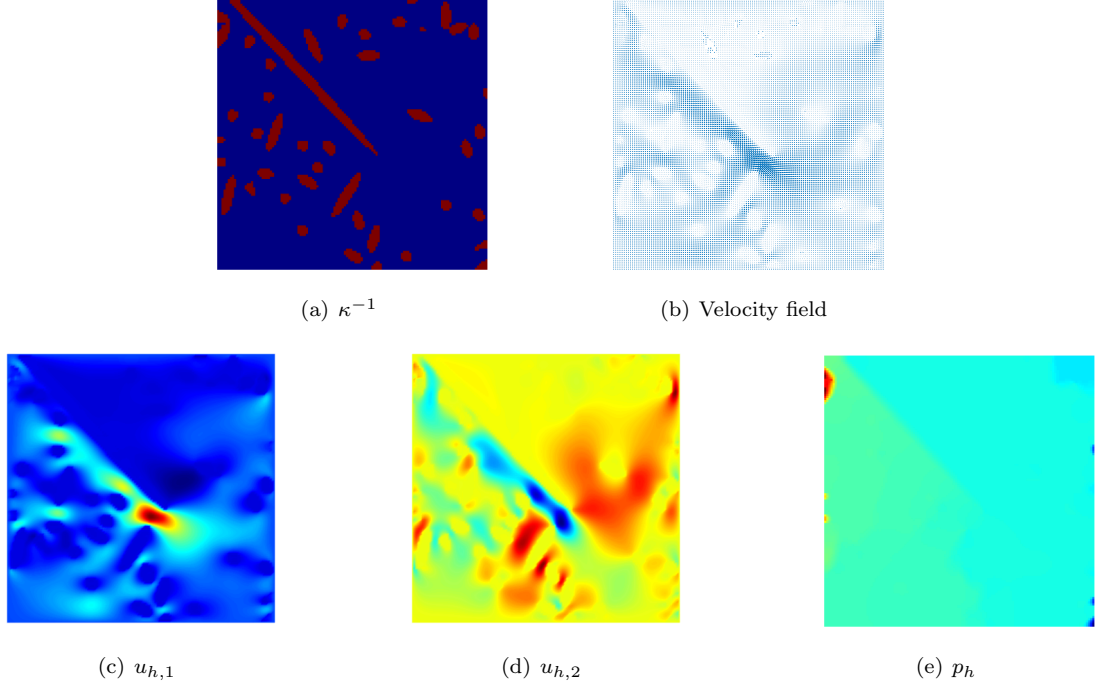


Fig. 6.2: Example 6.2: Numerical results. (a) Profile of κ^{-1} for fibrous structure; (b) Velocity field of \mathbf{u}_h ; (c) First component of velocity $u_{h,1}$; (d) second component of velocity $u_{h,2}$; (e) pressure profile p_h ;

The velocity fields of aforementioned tow examples are shown in Fig. 6.2(b) and Fig. 6.3(b). It is evident that the fluids both avoid regions of low permeability (the red part for κ^{-1}), and preferentially flow through the regions of high permeability (the blue part for κ^{-1}).

6.2. Numerical tests for a posteriori error estimate. In this subsection, we present two sets of examples to verify the reliability and Efficiency of the posteriori estimator η . Since the mesh is no longer a quasi-uniform polygonal mesh in our adaptive algorithm, the following numerical performance is reported with respect to the DOFs. Thus, the convergent rates of the error $(\nu^2 \|\mathbf{u} - \mathbf{u}_h\|^2 + \|p - p_h\|^2)^{1/2}$ and η are expected to be $\mathcal{O}(\text{DOFs}^{-1/2})$, where $h = \mathcal{O}(\text{DOFs}^{-1/2})$ for quasi-uniform mesh in two dimensions.

To measure the quality of the posteriori estimator, we define the effectivity index as

$$(6.2) \quad \text{Eff} := \left(\frac{\eta^2}{\text{Err}_{\mathbf{u}}^2 + \text{Err}_p^2} \right)^{1/2},$$

where

$$\text{Err}_{\mathbf{u}} := \nu \|\mathbf{u} - \mathbf{u}_h\| \quad \text{and} \quad \text{Err}_p = \|p - p_h\|.$$

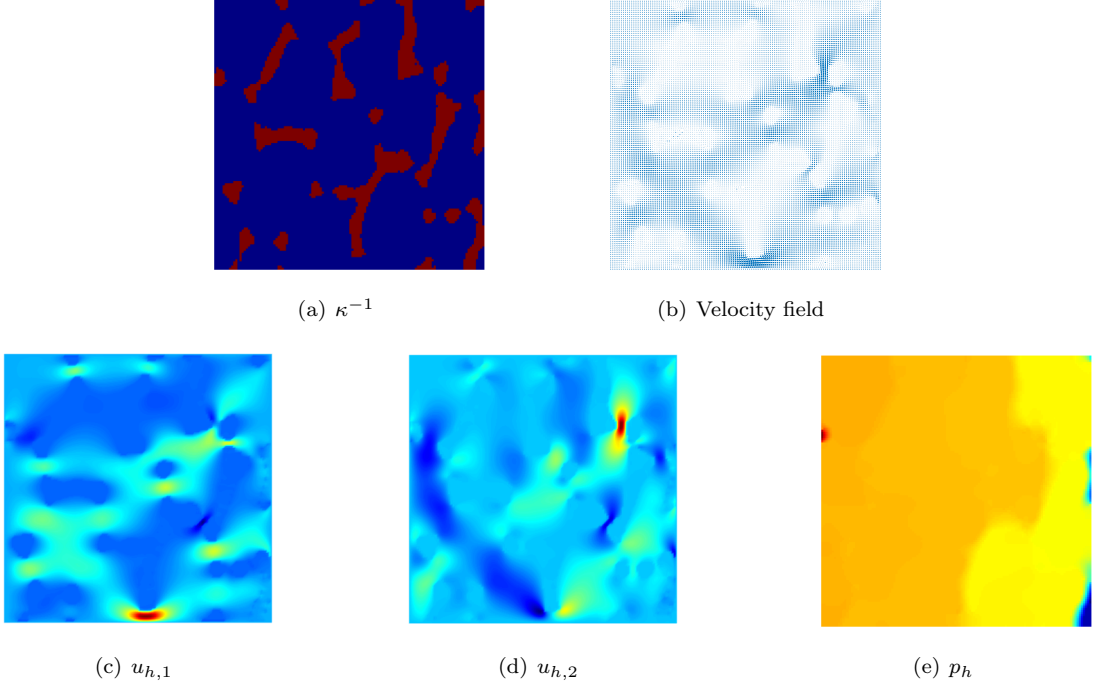


Fig. 6.3: Example 6.3: Numerical results. (a) Profile of κ^{-1} for fibrous structure; (b) Velocity field of \mathbf{u}_h ; (c) First component of velocity $u_{h,1}$; (d) Second component of velocity $u_{h,2}$; (e) Pressure profile p_h ;

EXAMPLE 6.4. The domain is $\Omega = (0, 1) \times (0, 1)$ and the exact solution is set to be

$$(6.3) \quad \mathbf{u} = \begin{pmatrix} 10x^2(1-x)^2y(1-y)(1-2y) \\ -10x(1-x)(1-2x)y^2(1-y)^2 \end{pmatrix}, \quad p = -10(2x-1)(2y-1),$$

where the load function \mathbf{f} is suitably chosen, and it is easy to check that $\nabla \cdot \mathbf{u} = 0$ and $(p, 1) = 0$. The marking parameter δ and tolerance tol are set equal to 0.4 and 10^4 , respectively. We carry out this test starting from the Voronoi base mesh shown in Fig 6.1(c), and set $\nu = 1e-2$, $\kappa^{-1} = 1$. After 13 iterations, the final results as shown in Table 6.2. Moreover, we can observe that the desired $\mathcal{O}(\text{DOFs}^{-1/2})$ optimal convergence rate is reached for both the error $(\text{Err}_{\mathbf{u}}^2 + \text{Err}_p^2)^{1/2}$ and estimator η . The efficiency index Eff is close to a constant from 7 to 8. These results validate our analytical predictions.

EXAMPLE 6.5. Consider the the exact solution as

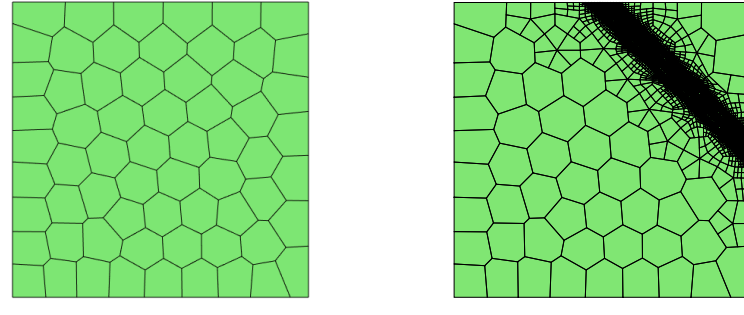
$$(6.4) \quad \mathbf{u} = -10^3 e^{-10^3(1.5-x-y)^2} \begin{pmatrix} 1 \\ -1 \end{pmatrix} \quad \text{and} \quad p = 2e^x \sin(y) \quad \text{in} \quad \Omega = (0, 1) \times (0, 1),$$

which is similar to that in [3]. Setting $\nu = 0.5$, $\kappa^{-1} = 0.01$ and the numbers of loop $\mathcal{L} = 22$. We emphasize that there exists a inner layer around the line $1.5 - x - y = 0$. We perform the test, and the numerical results as shown in Fig. 6.4. We can observe that the mesh refinement is concentrated around the line

Table 6.2: Example 6.4. the errors for a series of Voronoi meshes

DOFs	η	Rate	$(\text{Err}_{\mathbf{u}}^2 + \text{Err}_p^2)^{1/2}$	Rate	Eff
453	4.2849e+00	-	6.0318e-01	-	7.1038
1179	2.4851e+00	-0.57	3.3653e-01	-0.61	7.3846
6684	1.0189e+00	-0.51	1.2905e-01	-0.55	7.8949
13794	7.0928e-01	-0.50	8.8856e-02	-0.52	7.9823
28134	4.9559e-01	-0.50	6.2125e-02	-0.50	7.9772

$1.5 - x - y = 0$, which is consistent with the result we expected. We also notice that, looking at the experimental rates of convergence, the order $\mathcal{O}(\text{DOFs}^{-1/2})$ is observed for all the unknowns. Through calculating, the effective index tends to a constant.



(a) Initial mesh

(b) Refined mesh

(c) Convergence

(d) Efficiency

Fig. 6.4: Example 6.5: Numerical results. (a)Initial mesh; (b) Finally refined mesh.

EXAMPLE 6.6. We consider the Brinkman equation (1.1) in circular segment with radius 1 and angle $3\pi/2$, as shown in Fig. 6.5(a), and with homogeneous right-hand side. The normal and tangential velocity

on the straight parts of the boundary are imposed and no slip condition is enforced on the remaining walls, i.e.,

$$(6.5) \quad \mathbf{u} = \begin{cases} (0, 1)^\top & \text{on straight lids,} \\ (-1, 0)^\top & \text{on otherwise curved wall.} \end{cases}$$

The viscosity and permeability are taken by $1e - 3$ and $1e3$. We can notice that the boundary data of velocity is discontinuous. The velocity \mathbf{u} has discontinuities at the origin and two corners of the boundary. The so-called corner singularity appears where the straight lids meet the curved wall. Therefore, we expect the mesh refinement to be concentrated at the origin and two corners. After 15 iterations, the results are depicted in Fig. 6.5. We see that most of the elements are located at the origin and two corners, which confirms that our method captures the corner singularity. Moreover, Fig. 6.5(d)-6.5(e) show a good agreement between our numerical results and the benchmark data.

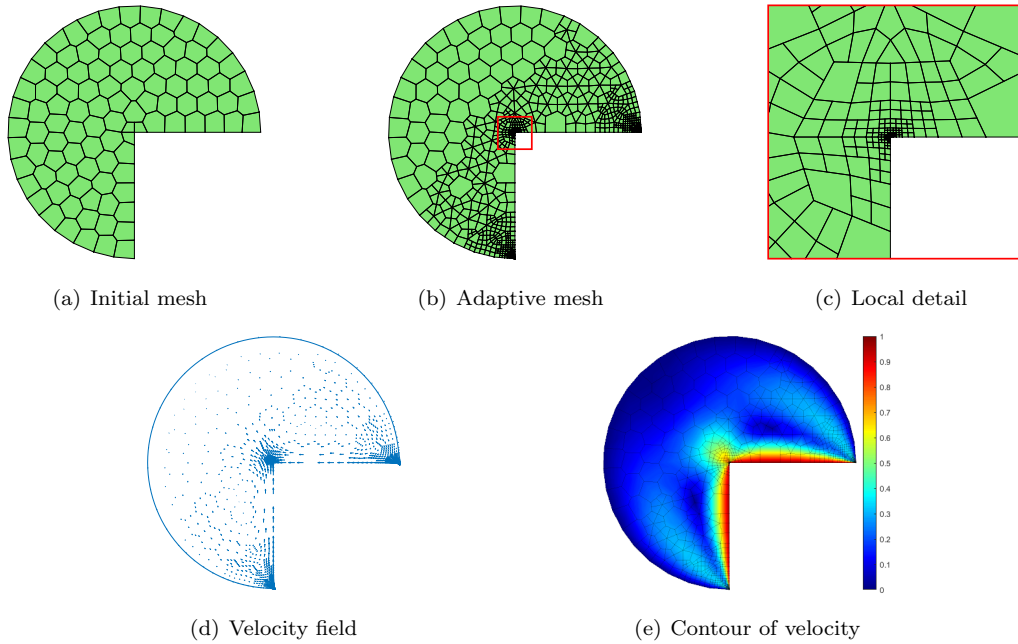


Fig. 6.5: Example 6.6: Numerical results. (a) Initial mesh; (b) Adaptive refined mesh; (c) Local Refined detail around origin; (d) Velocity field of \mathbf{u}_h ; (e) Contour plot of \mathbf{u}_h .

7. conclusion. In this paper, we have developed and analyzed a really pressure-robust VEM in solving the incompressible Brinkman equations. Based on the space divergence-preserving reconstructor \mathcal{R}_h , a well-posed VEM scheme is constructed. The velocity error in the energy norm and the pressure error in the L^2 norm are proven to be optimal. It should be emphasized that the velocity error does not explicitly depend on the pressure and even viscosity ν . Therefore, the locking phenomenon will not occur as $\nu \rightarrow 0$. To drive mesh adaptivity, we have designed a residual-based posteriori error indicator tailored for the Brinkman equations, and have demonstrated its effectiveness and reliability. Finally, some numerical experiments on three-type polygonal meshes are given to validate our theoretical analyses.

Acknowledgements. Yu Xiong was supported by Postgraduate Scientific Research Innovation Foundation of Xiangtan University (XDCX2024Y178). Yanping Chen was supported by the State Key Program of National Natural Science Foundation of China (11931003), Natural Science Research Start-up Foundation of Recruiting Talents of Nanjing University of Posts and Telecommunications (NY223127). This work is grateful to associate professor Gang Wang from Northwestern Polytechnical University for his constructive suggestions.

REFERENCES

- [1] Bashir Ahmad, Ahmed Alsaedi, Franco Brezzi, Lusia Donatella Marini, and Alessandro Russo. Equivalent projectors for virtual element methods. *Computers & Mathematics with Applications*, 66(3):376–391, 2013.
- [2] Paola Francesca Antonietti, Lourenço Beirão da Veiga, and Gianmarco Manzini. *The virtual element method and its applications*, volume 31. Springer Nature, 2022.
- [3] Tomás Barrios, Rommel Bustinza, Galina C García, and María González. An a posteriori error estimator for a new stabilized formulation of the Brinkman problem. In *Numerical Mathematics and Advanced Applications-ENUMATH 2013: Proceedings of ENUMATH 2013, the 10th European Conference on Numerical Mathematics and Advanced Applications, Lausanne, August 2013*, pages 253–261. Springer, 2015.
- [4] Lourenço Beirão da Veiga, Konstantin Lipnikov, and Gianmarco Manzini. Error analysis for a mimetic discretization of the steady Stokes problem on polyhedral meshes. *SIAM Journal on Numerical Analysis*, 48(4):1419–1443, 2010.
- [5] Lourenço Beirão da Veiga and Gianmarco Manzini. Residual a posteriori error estimation for the virtual element method for elliptic problems. *ESAIM: Mathematical Modelling and Numerical Analysis*, 49(2):577–599, 2015.
- [6] Lourenço Beirão da Veiga, Gianmarco Manzini, and Lorenzo Mascotto. A posteriori error estimation and adaptivity in hp virtual elements. *Numerische Mathematik*, 143(1):139–175, 2019.
- [7] Franco Brezzi and Michel Fortin. *Mixed and hybrid finite element methods*, volume 15. Springer Science & Business Media, 2012.
- [8] Erik Burman and Peter Hansbo. Stabilized Crouzeix–Raviart element for the Darcy–Stokes problem. *Numerical Methods for Partial Differential Equations: An International Journal*, 21(5):986–997, 2005.
- [9] Erik Burman and Peter Hansbo. A unified stabilized method for Stokes’ and Darcy’s equations. *Journal of Computational and Applied Mathematics*, 198(1):35–51, 2007.
- [10] Andrea Cangiani, Emmanuil Georgoulis, Tristan Pryer, and Oliver Sutton. A posteriori error estimates for the virtual element method. *Numerische Mathematik*, 137, 12 2017.
- [11] Long Chen and Jianguo Huang. Some error analysis on virtual element methods. *Calcolo*, 55:1–23, 2018.
- [12] Long Chen and Feng Wang. A divergence free weak virtual element method for the Stokes problem on polytopal meshes. *Journal of Scientific Computing*, 78:864–886, 2019.
- [13] Yanping Chen and Yu Xiong. A linearized BDF2 virtual element method for the unsteady Brinkman–Forchheimer equations with variable time step. *Chaos, Solitons & Fractals*, 187:115415, 2024.
- [14] Heng Chi, Lourenço Beirão da Veiga, and Glauco H Paulino. A simple and effective gradient recovery scheme and a posteriori error estimator for the virtual element method (VEM). *Computer Methods in Applied Mechanics and Engineering*, 347:21–58, 2019.
- [15] Lourenço Beirão da Veiga, Franco Brezzi, Andrea Cangiani, Gianmarco Manzini, Lusia Donatella Marini, and Alessandro Russo. Basic principles of virtual element methods. *Mathematical Models and Methods in Applied Sciences*, 23(01):199–214, 2013.
- [16] Lourenço Beirão da Veiga, Franco Brezzi, Lusia Donatella Marini, and Russo Alessandro. The virtual element method. *Acta Numerica*, 32:123–202, 2023.
- [17] Lourenço Beirão da Veiga, Franco Brezzi, Lusia Donatella Marini, and Alessandro Russo. The hitchhiker’s guide to the virtual element method. *Mathematical models and methods in applied sciences*, 24(08):1541–1573, 2014.
- [18] Lourenço Beirão da Veiga, Franco Dassi, and Giuseppe Vacca. Vorticity-stabilized virtual elements for the Oseen equation. *Mathematical Models and Methods in Applied Sciences*, 31(14):3009–3052, 2021.
- [19] Lourenço Beirão da Veiga, Carlo Lovadina, and Giuseppe Vacca. Divergence free Virtual Elements for the Stokes problem on polygonal meshes. *ESAIM Mathematical Modelling and Numerical Analysis*, 51, 2017.
- [20] Lourenço Beirão da Veiga, Carlo Lovadina, and Giuseppe Vacca. Divergence free Virtual Elements for the Stokes problem on polygonal meshes. *ESAIM Mathematical Modelling and Numerical Analysis*, 51:509 – 535, 10 2017.
- [21] Derk Frerichs-Mihov and Christian Merdon. Divergence-preserving reconstructions on polygons and a really pressure-robust virtual element method for the Stokes problem. *IMA Journal of Numerical Analysis*, 42, 2020.
- [22] Jixiao Guo, Yanping Chen, Jianwei Zhou, and Yunqing Huang. The virtual element method for solving two-dimensional fractional cable equation on general polygonal meshes. *International Journal of Computer Mathematics*, 0(0):1–21, 2023.
- [23] Diego Irisarri and Guillermo Hauke. Stabilized virtual element methods for the unsteady incompressible Navier–Stokes equations. *Calcolo*, 56(4):38, 2019.
- [24] Volker John, Alexander Linke, Christian Merdon, Michael Neilan, and Leo G. Rebholz. On the divergence constraint in mixed finite element methods for incompressible flows. *SIAM Review*, 59(3):492–544, 2017.
- [25] Yang Li, Yanhong Bai, and Minfu Feng. A stabilized Crank–Nicolson virtual element method for the unsteady Navier–Stokes problems with high Reynolds number. *Numerical Algorithms*, 1:39, 2023.
- [26] Xin Liu, Rui Li, and Yufeng Nie. A divergence-free reconstruction of the nonconforming virtual element method for

the Stokes problem. *Computer Methods in Applied Mechanics and Engineering*, 372:113351, 2020.

[27] Xin Liu and Yufeng Nie. Pressure-independent velocity error estimates for (Navier-) Stokes nonconforming virtual element discretization with divergence free. *Numerical Algorithms*, 90(2):477–506, 2022.

[28] Gianmarco Manzini and Annamaria Mazzia. A posteriori error analysis and mesh adaptivity for a virtual element method solving the Stokes equations. *Mathematics and Computers in Simulation*, 221:19–38, 2024.

[29] Lorenzo Mascotto. The role of stabilization in the virtual element method: A survey. *Computers & Mathematics with Applications*, 151:244–251, 2023.

[30] Jian Meng, Lourenço Beirão da Veiga, and Lorenzo Mascotto. Stability and interpolation properties for Stokes-like virtual element spaces. *Journal of Scientific Computing*, 94, 2023.

[31] Jian Meng, Liquan Mei, and Mingfa Fei. H^1 -conforming virtual element method for the Laplacian eigenvalue problem in mixed form. *Journal of Computational and Applied Mathematics*, 436:115395, 2024.

[32] David Mora, Gonzalo Rivera, and Rodolfo Rodríguez. A posteriori error estimates for a virtual element method for the Steklov eigenvalue problem. *Computers & Mathematics with Applications*, 74(9):2172–2190, 2017. Advances in Mathematics of Finite Elements, honoring 90th birthday of Ivo Babuška.

[33] Lin Mu, Junping Wang, and Xiu Ye. A stable numerical algorithm for the Brinkman equations by weak Galerkin finite element methods. *Journal of Computational Physics*, 273:327–342, 2014.

[34] Cameron Talischi, Glaucio H Paulino, Anderson Pereira, and Ivan FM Menezes. Polymesher: a general-purpose mesh generator for polygonal elements written in matlab. *Structural and Multidisciplinary Optimization*, 45:309–328, 2012.

[35] Giuseppe Vacca. An H^1 -conforming virtual element for Darcy and Brinkman equations. *Mathematical Models and Methods in Applied Sciences*, 28(01):159–194, 2018.

[36] N Verma and S Kumar. Lowest order virtual element approximations for transient Stokes problem on polygonal meshes. *Calcolo*, 58(4):48, 2021.

[37] Gang Wang, Lin Mu, Ying Wang, and Yinnian He. A pressure-robust virtual element method for the Stokes problem. *Computer Methods in Applied Mechanics and Engineering*, 382:113879, 2021.

[38] Gang Wang, Ying Wang, and Yinnian He. A posteriori error estimates for the virtual element method for the Stokes problem. *Journal of Scientific Computing*, 84, 2020.

[39] Gang Wang, Ying Wang, and Yinnian He. Two robust virtual element methods for the Brinkman equations. *Calcolo*, 58(4):49, 2021.

[40] Yang Wang, Huaming Yi, Xiaohong Fan, and Guanrong Li. Unconditionally optimal error estimates of linearized Crank-Nicolson virtual element methods for quasilinear parabolic problems on general polygonal meshes. *ESAIM: Mathematical Modelling and Numerical Analysis*, 58:881 – 926, 03 2024.

[41] Ying Wang, Gang Wang, and Yue Shen. A pressure-robust virtual element method for the Navier-Stokes problem on polygonal mesh. *Computers & Mathematics with Applications*, 131:124–137, 2023.

[42] Ying Wang, Gang Wang, and Feng Wang. An adaptive virtual element method for incompressible flow. *Computers & Mathematics with Applications*, 101:63–73, 2021.

[43] Xiaoping Xie, Jinchao Xu, and Guangri Xue. Uniformly-stable finite element methods for Darcy-Stokes-Brinkman models. *Journal of Computational Mathematics*, pages 437–455, 2008.

[44] Yu Xiong, Yanping Chen, Jianwei Zhou, and Qin Liang. Divergence-free virtual element method for the Stokes equations with damping on polygonal meshes. *NUMERICAL MATHEMATICS-THEORY METHODS AND APPLICATIONS*, 17(1):210–242, 2024.

[45] Xiu Ye and Shangyou Zhang. A stabilizer free weak Galerkin finite element method on polytopal mesh: Part ii. *Journal of Computational and Applied Mathematics*, 394:113525, 2021.

[46] Y. Yu. mvem: Matlab programming for virtual element methods, 2019–2022.

[47] Qilong Zhai, Ran Zhang, and Lin Mu. A new weak Galerkin finite element scheme for the Brinkman model. *Communications in Computational Physics*, 19(5):1409–1434, 2016.

[48] Jikun Zhao, Bei Zhang, Shipeng Mao, and Shaochun Chen. The nonconforming virtual element method for the darcy–stokes problem. *Computer Methods in Applied Mechanics and Engineering*, 370:113251, 2020.

[49] Jikun Zhao, Wenhao Zhu, Bei Zhang, and Yongqin Yang. The stabilized nonconforming virtual element method for the darcy–stokes problem. *Communications in Nonlinear Science and Numerical Simulation*, 138:108252, 2024.